



# **JGR Space Physics**

#### RESEARCH ARTICLE

10.1029/2022JA030331

#### **Key Points:**

- Some radial transport mechanisms produce drift phase structure
- Drift phase structure is not strongly associated with electron belt
- Drift resonance with random-phase broadband waves appears to dominate

#### Correspondence to:

T. P. O'Brien, paul.obrien@aero.org

#### Citation:

O'Brien, T. P., Green, J. C., Halford, A. J., Kwan, B. P., Claudepierre, S. G., & Ozeke, L. G. (2022). Drift phase structure implications for radiation belt transport. *Journal of Geophysical Research: Space Physics*, *127*, e2022JA030331. https://doi.org/10.1029/2022JA030331

Received 27 JAN 2022 Accepted 1 JUL 2022

#### **Author Contributions:**

**Conceptualization:** J. C. Green, A. J. Halford, S. G. Claudepierre, Louis G. Ozeke

Formal analysis: J. C. Green, A. J. Halford

**Investigation:** J. C. Green, A. J. Halford, B. P. Kwan

Methodology: J. C. Green, A. J. Halford, S. G. Claudepierre, Louis G. Ozeke Software: J. C. Green, A. J. Halford Validation: J. C. Green Visualization: A. J. Halford Writing – review & editing: J. C. Green, S. G. Claudepierre, Louis G. Ozeke

© 2022 American Geophysical Union. All Rights Reserved.

# **Drift Phase Structure Implications for Radiation Belt Transport**

T. P. O'Brien<sup>1</sup>, J. C. Green<sup>2</sup>, A. J. Halford<sup>1,3</sup>, B. P. Kwan<sup>1</sup>, S. G. Claudepierre<sup>1,4</sup>, and Louis G. Ozeke<sup>5</sup>

<sup>1</sup>Space Sciences Department, The Aerospace Corporation, El Segundo, CA, USA, <sup>2</sup>Space Hazards Applications, LLC, Golden, CO, USA, <sup>3</sup>Now at NASA Goddard Spaceflight Center, Greenbelt, MD, USA, <sup>4</sup>Now at University of California, Los Angeles, CA, USA, <sup>5</sup>Department of Physics, University of Alberta, Edmonton, AB, Canada

**Abstract** We examine drift phase structure in the electron radiation belt observations to differentiate radial transport mechanisms. Impulsive electrostatic or electromagnetic fields can cause radial transport and produce drift echoes (periodic drift phase structures with energy-dependent period). Narrow-band standing electromagnetic wave fields can also cause radial transport, while producing energy-independent periodic drift phase structures. Broad-band, random-phase electromagnetic wave fields can cause radial transport, but do not necessarily produce drift phase structure. We present results of three case studies showing little association between drift phase structure and approximately MeV electron flux enhancements in the outer belt. We estimate the amplitude of drift phase structures expected for impulsive or narrow-band interactions to compete with broad-band, random-phase waves. We show that the observed drift phase structure is typically much smaller than would be present if either impulses or narrow-band waves were the dominant cause of radial transport. We conclude that radial transport is primarily consistent with the broad-band, random-phase, small perturbations assumed in quasilinear diffusion theory, although we cannot rule out the unlikely possibility that radial transport plays little role in radiation belt dynamics.

Plain Language Summary Radial motion of electrons is one of the most significant processes in the dynamics of the Earth's electron radiation belts. We examine the ripples in the time series of radiation belt electron flux observations to determine how the electrons move radially in space. Different kinds of radial motion leave different signatures in these time series ripples. Large ripples are rare enough that much of the radial reshaping of the radiation belts occurs independent of their influence. Established radial transport theory, known as quasilinear theory, is consistent with many small ripples, but our analysis cannot rule out the unlikely alternative that the small ripples indicate that there is little or no radial transport happening in the radiation belts.

#### 1. Introduction

Radial transport of electrons has long been thought to be an essential component of radiation belt dynamics (Falthammar, 1965; 1968). It can be an energization mechanism, when it brings particles from the plasma sheet into the radiation belts while preserving their first and second adiabatic invariants (e.g., Jaynes et al., 2018; Ozeke et al., 2019). It can also be a loss mechanism, transporting particles outward through the magnetopause (Loto'aniu et al., 2010; Ozeke et al., 2020; Shprits et al., 2006). While the relevance of transport is apparent, the details of how it occurs and is modeled are still debated. Although radial transport is sometimes clearly impulsive (e.g., Foster et al., 2015; Hao et al., 2019; Hudson et al., 2017, 2020; Li et al., 1993; Kress et al., 2007; Patel et al., 2019), it is most often represented as a diffusive process in radiation belt simulations (Boscher et al., 1996; Brautigam & Albert, 2000; Elkington et al., 2003; Fei et al., 2006; Glauert et al., 2014; Loto'aniu et al., 2006; Ozeke et al., 2020; Reeves et al., 2012; Shprits & Thorne, 2004; Su et al., 2011; Subbotin & Shprits, 2009; Tu et al., 2013). In these simulations, radial transport is modeled as diffusive changes in  $L^*$ , a form of the third adiabatic invariant associated with azimuthal particle drift around Earth. Some test particle simulations have been used to assess the validity of this representation and support the use of this diffusive approximation (e.g., Huang et al., 2010; Li et al., 2016; Sarris et al., 2006). However, results from other test particle simulations argue that radial transport is idiosyncratic to each individual geomagnetic storm, and the diffusive approximation only holds in aggregate over many storms (Chen et al., 1992, Riley & Wolf, 1992, Ukhorskiy et al., 2006; Ukhorskiy and

O'BRIEN ET AL. 1 of 19

Our goal is to distinguish what general type of transport (diffusive vs. nondiffusive) occurs during radiation belt enhancements using the drift phase structure of the electron flux as a diagnostic tool. Additionally, we will use the drift structure to characterize the details of the transport process and discern between radial transport events caused by impulsive injections and those related to interaction with ultra-low frequency (ULF) waves. To do so requires an understanding of the signatures of each of these processes.

Electrostatic and electromagnetic impulses produce drift phase structure of the electron flux known as drift echoes (Brewer et al., 1969; Lanzerotti et al., 1969; Schulz, 1991; Schulz & Lanzerotti, 1974). These drift echoes are characterized by fluctuations with a period that corresponds to the particle's drift period. Since the drift period depends on the particle energy, the hallmark of impulsive transport is energy-dispersed drift echoes. Of course, if enough impulses are randomly superimposed on each other within a single drift period, no drift echoes can be observed. However, in this scenario, the impulsive behavior is effectively indistinguishable from the action of broad-band, random-phase power and the diffusive approximation is clearly applicable.

Narrow-band standing electromagnetic waves produce oscillations in particle drift phase structures. In this case, all energies oscillate at the same frequency, but there is an energy-dependent phase shift (Chen et al., 2017; Claudepierre et al., 2013; Hao et al., 2020; Kokubun et al., 1977; Southwood & Kivelson, 1981; Teramoto et al., 2019; Zong et al., 2009). A superposition of many narrow-band waves can smooth out the drift phase structure (Elkington et al., 2003), but, again, this is effectively indistinguishable from broad-band, random-phase power, and the diffusive approximation would be applicable. In fact, a variety of interactions are possible, involving broad and narrow-band waves, with global and limited local time scope (see, e.g., Hao et al., 2019, 2020; Zhao et al., 2021).

In the quasilinear approximation (Falthammar, 1965) of diffusion, broad-band, random-phase, small amplitude waves produce many infinitesimal radial transport events over the course of a particle's drift orbit. As this approximation breaks down, either due to large amplitude waves, nonrandom phase, or narrow-band power, drift phase structure should become more evident.

Using multiple case studies, we will look for evidence in the electron drift-phase structure of nonquasilinear, nondiffusive processes leading to significant transport. We adopt as our null hypothesis that the radial transport is diffusive even on timescales as short as a few hours. We will reject the null hypothesis if, during radiation belt enhancements, we can detect drift phase structures that are often larger than those expected from the quasilinear approximation. Section 2 describes our method for determining the amplitude of drift phase structures that would indicate nondiffusive transport. Section 3 describes the radiation belt data used in the analysis. Section 4 describes the individual events considered. Lastly, Section 5 concludes that the null hypothesis stands: observed drift phase structures are rarely larger than what is implied by quasilinear diffusion, even in storms that appear to have significant radial transport.

#### 2. Estimating the Size of Drift Phase Structure

Our null hypothesis is that diffusive quasilinear radial transport, which preserves the first and second adiabatic invariants, is the dominant transport process in the radiation belts. Since diffusive transport is caused by the superposition of many waves or impulses, we expect this type of transport to create some level of fluctuations in the particle flux. In order to differentiate diffusive from non-diffusive transport we must estimate the threshold size (amplitude) of drift phase structures that would indicate non-quasilinear transport. To make this size estimate, we begin with the transport equation:

$$\frac{\partial \overline{f}}{\partial t} = L^2 \frac{\partial}{\partial L} \Big|_{M,K} \left[ \frac{D_{LL}}{L^2} \frac{\partial \overline{f}}{\partial L} \Big|_{M,K} \right]$$
 (1)

O'BRIEN ET AL. 2 of 19

In this equation  $\overline{f}$  is the phase-averaged phase space density (PSD), and the coordinates are adiabatic invariants (e.g., Schluz and Lanzerotti, 1974):

$$M = \frac{p^2 \sin^2 \alpha}{2m_0 B} \tag{2}$$

$$K = \int_{s_m^{\prime}}^{s_m} \sqrt{B_m - B(s)} ds \tag{3}$$

$$L = L^* = \frac{2\pi\mu_E}{R_E\Phi} \tag{4}$$

M is the first invariant, which depends on the particle's momentum p, local pitch angle  $\alpha$ , rest mass  $m_0$ , and the local magnetic field strength B. K is the second invariant, which involves an integral of the local field strength B(s) relative to the mirror point field strength  $B_m$ , with the integral taken along the field line from the southern  $(s_m)$  to northern  $(s_m)$  mirror points. Finally, the third invariant L depends on the magnetic moment of the Earth  $(\mu_E)$ , Earth's radius  $(R_E)$ , and the magnetic flux  $\Phi$  enclosed by the particle's drift orbit. For our analysis, we will use the TS04D global magnetic field model (Tsyganenko & Sitnov, 2005) to provide K and L. However, as the radial diffusion coefficients are computed in a combination of quiet field models, we will use the Olson-Pfitzer Quiet field model (OPQ: Olson & Pfitzer, 1977) to identify the spacecraft location and the L parameter for local  $D_{LL}$ . Both because of the use of quiet field models in capturing  $D_{LL}$  and because ULF waves do not follow particle drift trajectories, we cannot, at this time, make better use of the more realistic TS04D field model.

#### 2.1. Diffusion Coefficient and Drift Phase Structure

The amount of transport in Equation 1 is captured in the diffusion coefficient,  $D_{LL}$ , and is the focus of our derivation of the size of diffusive and nondiffusive drift structure. It is given by:

$$D_{LL} = \frac{\left\langle (\Delta L)^2 \right\rangle}{2\Delta t} \tag{5}$$

In essence,  $D_{LL}$  arises from a series of wave-particle interactions, separated in time by  $\Delta t$ , that produce changes in L that have a variance  $\langle (\Delta L)^2 \rangle$  over many interactions. If these perturbations conserve PSD (Liouville's theorem) then the PSD amplitude can be related to how far they moved  $(\Delta L)$  and the radial gradient in PSD  $\frac{\partial \overline{f}}{\partial L}\Big|_{M,K}$ . The quasilinear regime is defined by many such perturbations (small  $\Delta t$ ) that are small in amplitude (small  $\langle (\Delta L)^2 \rangle$ ) producing a finite DLL.

Schulz and Lanzerotti (1974, section IV.8) estimate an electromagnetic  $D_{LL}$  based on magnetic impulses that might be appropriate for quiet time. Their treatment is especially interesting because it derives  $D_{LL}$  from the peak-to-peak amplitude of drift echoes. Our estimate of the expected amplitude of drift phase structures applies the same logic, but in reverse—starting from  $D_{LL}$ , how large in amplitude should the drift phase structures be to indicate transport in excess of the quasilinear approximation?

We begin our estimate of the expected size of drift phase structure by assuming an initial state in which the PSD is sufficiently mixed in drift phase such that  $f_0(M, K, L, \phi_3) = \overline{f}_0(M, K, L)$ , where  $\phi_3$  is the drift phase angle and  $f_0$  has been averaged over bounce- and gyro-phases. We then assume the PSD is perturbed by an interaction with some unspecified electric and magnetic fields that preserve M and K, but induce a  $\phi_3$ -dependent change in L. We denote this change  $\Delta L(\phi_3)$ , which is the change in L as a function of  $\phi_3$  after the interaction. Conservation of phase-space density (Liouville's theorem) provides that the PSD after the interaction is:

$$f_1(M, K, L, \phi_3) = \overline{f}_0(M, K, L - \Delta L(\phi_3))$$

$$\tag{6}$$

Figure 1 illustrates this process: the particles carry their initial phase-space density with them as they move in L. Drift phase structure arises because the displacement is phase-dependent. The size of the drift phase structure depends on the displacement in L and the local phase space density gradient (for a statistical investigation of this phenomenon, see Sarris et al., 2021). As noted by Hartinger et al. (2020) if there is no radial gradient in the phase

O'BRIEN ET AL. 3 of 19

21699402, 2022, 8, Downloaded from https://agupubs.onlinelibrary.wiley.com/doi/10.1029/2021A030331 by University Of Athens, Wiley Online Library on [29/11/2023]. See the

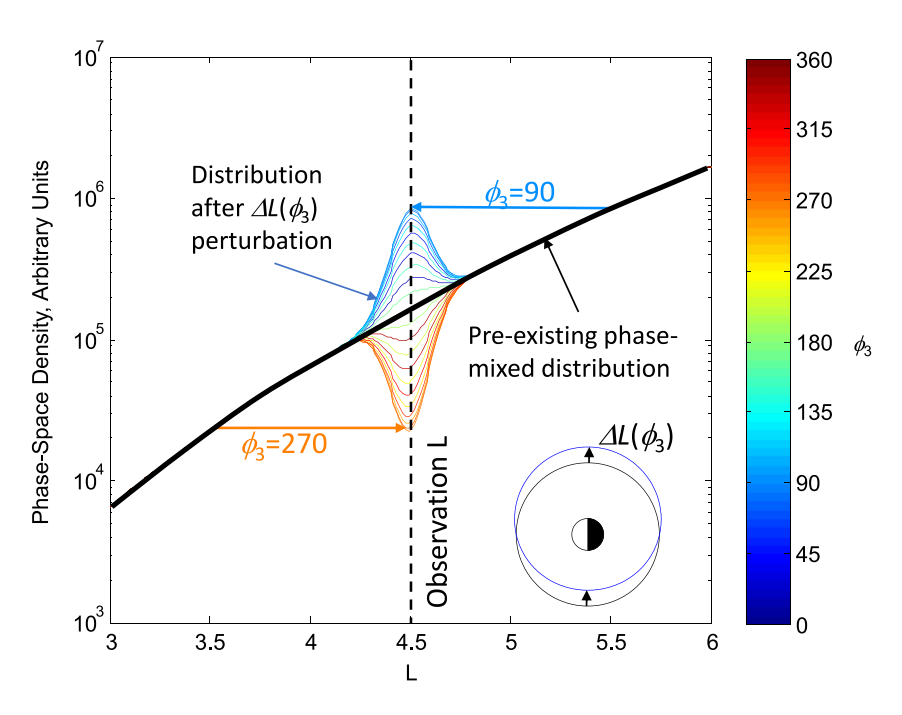


Figure 1. An illustration of how a radial offset that depends on drift phase can lead to drift phase structure. Particles at  $\phi_3 \sim 90^\circ$  are transported inward, and those at  $\phi_3 \sim 270^\circ$  are transported outward (see inset). Liouville's theorem says that they carry their phase space density (PSD) with them along their trajectories. This results in smooth, phase-mixed prior distribution producing a phase-dependent PSD at L=4.5.

space density, radial transport will not result in drift phase structures, including drift echoes; this is common in the outer zone at ~MeV energies. We must, therefore, be careful to account for the presence or absence of a PSD gradient when assessing the expected size of drift phase structure for quasilinear diffusion.

Taking a natural logarithm of Equation 6 and the using a first order Taylor expansion yields:

$$\ln f_1(M, K, L, \phi_3) \cong \ln \overline{f}_0(M, K, L) - \frac{\partial \ln \overline{f}_0}{\partial L} \Big|_{M, K} \Delta L(\phi_3)$$
 (7)

The PSD gradient  $\frac{\partial \ln \overline{f}_0}{\partial L}\Big|_{M,K}$  emerges explicitly in the second term of the Taylor expansion.

If we take a drift average  $(\langle \cdot \rangle_d)$ , we have

$$\ln \overline{f}_{1}(M, K, L) = \left\langle \ln f_{1}(M, K, L, \phi_{3}) \right\rangle_{d} \cong \ln \overline{f}_{0}(M, K, L) - \frac{\partial \ln \overline{f}_{0}}{\partial L} \Big|_{M, K} \left\langle \Delta L(\phi_{3}) \right\rangle_{d} \tag{8}$$

The variance is:

$$\left\langle (\Delta \ln f)^2 \right\rangle_d = \left\langle \left[ \ln f_1(M, K, L, \phi_3) - \ln \overline{f}_1(M, K, L) \right]^2 \right\rangle_d \cong \left( \frac{\partial \ln \overline{f}_0}{\partial L} \Big|_{M, K} \right)^2 \left\langle (\Delta L (\phi_3))^2 \right\rangle_d \tag{9}$$

Over many interactions,  $\langle (\Delta L(\phi_3))^2 \rangle_d$  should converge to  $\langle (\Delta L)^2 \rangle$  (i.e., the population variance). Thus, we have

$$\left\langle (\Delta \ln f)^2 \right\rangle_d \sim \left( \frac{\partial \ln \overline{f}_0}{\partial L} \Big|_{M,K} \right)^2 \left\langle (\Delta L)^2 \right\rangle = \left( \frac{\partial \ln \overline{f}_0}{\partial L} \Big|_{M,K} \right)^2 2\Delta t D_{LL} \tag{10}$$

While this approximation does not hold instantaneously, it does describe the expected magnitude of perturbations for  $D_{LL}$  made up of individual perturbation episodes. Left open to interpretation is the time between perturbations,  $\Delta t$ . If  $\Delta t$  is small compared to a drift period,  $\tau_d$ , then the system is clearly in the quasilinear diffusive regime

O'BRIEN ET AL. 4 of 19

(many interactions per drift period). However, for values of  $\Delta t$  that are comparable to or larger than  $\tau_d$ , the system may deviate from the quasilinear ideal. Thus, a signature of the system deviating from the quasilinear regime is

$$\left\langle (\Delta \ln f)^2 \right\rangle_d > \left( \frac{\partial \ln \overline{f}_0}{\partial L} \Big|_{M,K} \right)^2 2\tau_d D_{LL}$$
 (11)

when  $D_{LL}$  is given by the quasilinear approximation. In other words, this expression sets a floor on the size of drift phase perturbations one would expect to observe if significant nonquasilinear behavior is present. We cannot observe the statistics of the process directly because nature does not provide repeated experiments the way a laboratory does. However, we know that the condition in Equation 11 can only be met, if there are sufficient cases of

$$\left| \ln f_1(M, K, L, \phi_3) - \ln \overline{f}_1(M, K, L) \right| > \left| \frac{\partial \ln \overline{f}_0}{\partial L} \right|_{M, K} \left| \sqrt{2\tau_d D_{LL}} \right|$$
(12)

In words, the detrended phase space density, or flux, must exceed the L gradient times the expected L displacement on a drift timescale, in a root-mean-squared sense. To use Equation 12 requires an estimate of  $D_{LL}$  from quasilinear theory. There have been many attempts to specify the diffusion coefficient (Ali et al., 2015, 2016; Brautigam & Albert, 2000; Brautigam et al., 2005; Cornwall, 1968, 1972; Fei et al., 2006; Huang et al., 2010; Lanzerotti et al., 1970, 1978; Lanzerotti & Morgan, 1973; Lanzerotti & Wolfe, 1980; Lejosne et al., 2013; Li et al., 2016; Ozeke et al., 2012, 2014). We highlight the work of Fei et al. (2006) for a discussion of the challenges in relating conceptual representations of the electric and magnetic components of  $D_{LL}$  to practical observations of in situ electromagnetic fields. Ultimately, we adopt the  $D_{LL}$  representation of Ozeke et al. (2014) as it is based on the most comprehensive ULF wave observations. They combined ground-based and space-based magnetometer data. The electric field ULF power was estimated by mapping ground-based magnetometer data up the field line using an Alfvén wave approximation in a dipole field. The magnetic field ULF power was obtained from compressional fields measured at in situ near the magnetic equator throughout the outer zone.

Next, we relate the statement about phase-space density drift phase structure in Equation 12 to observed drift phase structure in particle flux.

#### 2.2. Drift Phase Structure in Observed Fluxes

A satellite typically observes flux,  $j = p^2 f$ , as a function of energy (or, equivalently, p), local pitch angle ( $\alpha$ ), and time t. From the satellite location  $\vec{r}$ , the channel energy, and look direction, and the TS04D global magnetic field model, we can infer the M, K, L, and  $\phi_3$  coordinates of particles being measured at any time. Thus, we can write:

$$j(p,\alpha,\vec{r}) = p^2 f(M(p,\alpha,\vec{r}), K(\alpha,\vec{r}), L(\alpha,\vec{r}), \phi_3(p,\alpha,\vec{r}))$$
(13)

So long as the spacecraft is not moving too fast, we can safely assume that a time average in an energy-pitch angle bin over a drift period along the spacecraft motion is equivalent to a drift average at fixed M, K, and L. That is, in terms of natural logs:

$$\left\langle \ln j \left( p, \alpha, \vec{r}(t) \right) \right\rangle_{\tau_d} \approx 2 \ln p + \left\langle \ln f \left( M, K, L, \phi_3 \right) \right\rangle_d$$
 (14)

With minor manipulations, we can then show that Equation 12 becomes:

$$\left| \ln j \left( p, \alpha, \vec{r}(t) \right) - \overline{\ln j} \left( p, \alpha, \vec{r}(t) \right) \right| > \left| \frac{\partial \ln \overline{f}_0}{\partial L} \right|_{M,K} \left| \sqrt{2\tau_d D_{LL}} = \Delta \ln j \right|$$
 (15)

Here  $\overline{\ln j}$  represents a centered time average taken over at least one drift period. Appendix A provides the procedure for computing  $\frac{\partial \ln \overline{f_0}}{\partial L}$  from flux observations. With Equation 15 in hand, we have a tool for relating observed drift phase structure in particle fluxes to the amplitudes  $\Delta \ln j$  of the drift phase structures that would be required for nonquasilinear radial transport to dominate over quasilinear radial transport.

O'BRIEN ET AL. 5 of 19

21699402, 2022, 8, Downloaded from https://agupubs.onlinelibrary.wiley.com/doi/10.1029/2022/A030331 by University Of Athens, Wiley Online Library on [29/11/2023]. See the Terms

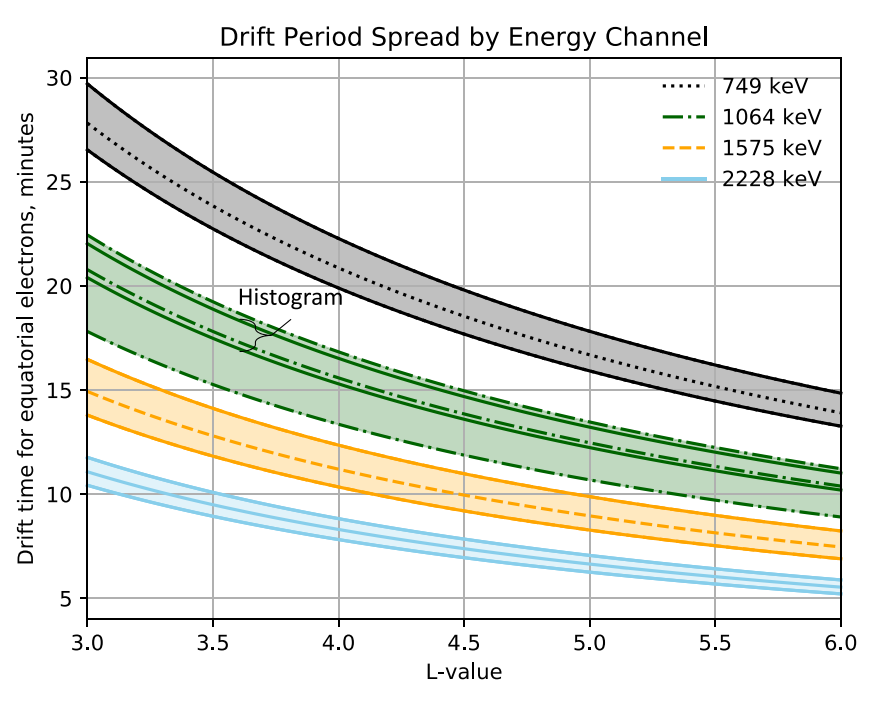


**Figure 2.** The *L*-dependence and bandwidth of the dipole drift period for the MagEIS electron energy channels used in this study. The 1,064 keV channel is used as a broader main rate and a narrower histogram channel. The other three channels are only used in their main rate form. The color-filled bandwidth represents the full-width, half-max channel response. The drift period assumes equatorially mirroring electrons.

#### 3. Data Sources

Our analysis relies on several data sources: in situ particles and fields, a geomagnetic activity index, and ground magnetometers. The in-situ particle and fields come from the *B* spacecraft in NASA's Van Allen Probes mission (Mauk et al., 2013), abbreviated RBSP, for Radiation Belt Storm Probes, its pre-launch designator. The vehicle was in a low inclination orbit, with a roughly 9-hr orbit, having low altitude inclination and an apogee of around 5.8 R<sub>E</sub>. The vehicle spin was approximately 5.5 RPM on an axis that was roughly pointed sunward. The elliptical, low-inclination orbit allowed RBSP-B to sweep through the entire outer radiation belt in a few hours, and it repeated this process twice each orbit, once outbound, and once inbound.

We use the electron flux from the Magnetic Electron Ion Spectrometer (MagEIS) family of sensors (Blake et al., 2013) on RBSP. We use the level 3 data product (release 4), which includes electron flux versus time, energy, and local pitch angle. Every approximately 11 s, there is 2-dimensional record providing flux at fixed energies and local pitch angles. The pitch angle bins are about 15° wide, while the energy bins vary across the sensor range, and energy resolution at approximately 1 MeV is 10%–30% full-width-half-max (FWHM). Figure 2 shows how drift period depends on *L*, and how this energy spread translates to spread in drift period for particles in each of the four energy channels we will use. Although MagEIS provides a background-corrected flux for most energy channels much of the time, we use uncorrected fluxes because they are always available, and we are working in a region of the outer zone where backgrounds are not large. We also examine MagEIS histogram data products (Claudepierre et al., 2021) which have narrow energy bandwidth, and so provide a potentially sharper view of drift phase structures with larger amplitudes (see, e.g., Hartinger et al., 2018; Sarris et al., 2020). In particular, we select a histogram channel whose nominal energy is close to the center energy of the main channel for the same pixel so that its flux is directly comparable, with only the energy bandwidth being different.

For context, we examine magnetometer data from the Electric and Magnetic Field Instrument Suite and Integrated Science (EMFISIS) instrument (Kletzing et al., 2013) on RBSP-B. We use a 1-s, level 3 product, which provides magnetometer vectors in the geocentric solar magnetospheric (GSM) coordinate system, with accuracy and resolution of better than 1 nT.

O'BRIEN ET AL. 6 of 19

We use the ground-based planetary Kp index as inputs to the Ozeke et al. (2014) model of  $D_{LL}$ . We use the Omni database for Kp and hourly interplanetary and geomagnetic conditions (King & Papitashvili, 2005). We also use ground-based magnetometry from the Canadian Array for Realtime Investigations of Magnetic Activity (CARISMA) network (Mann et al., 2008) to compute event-specific  $D_{LL}$ . The general procedure for computing  $D_{LL}$  is based on Ozeke et al. (2014), whereas the details of computing event-specific  $D_{LL}$  are given in Mann et al. (2016) and Ozeke et al. (2017, 2020).

We use these data sets together to examine three magnetic storm events to determine whether the observed drift phase structure in the outer zone is large enough to indicate nonquasilinear radial transport is a significant contributor to outer zone dynamics.

# 4. Event Study

Because every geomagnetic storm is unique (see, e.g., Reeves et al., 2003), it is necessary to look at several events to gain a sense of whether and how the drift phase structure indicates radial transport is happening. We consider three different events, chosen from a manual survey of all RBSP passes in 2013 for data quality (availability, low Poisson noise) and exemplary drift-phase structure. As such, if there is a selection bias, it is most likely in favor of larger drift-phase structure (i.e., more likely to reject the null hypothesis). For each event, we provide an overview of geomagnetic conditions and MagEIS observations in time series form. We then slice each event into individual RBSP-B passes through the outer zone. For each pass, we detrend the fluxes to isolate the drift-phase structure. We also compute the expected magnitude of that drift-phase structure, according to Equation 15. We provide the analysis details during the exposition on the first event and will follow the same analysis procedure for the second and third events. We then examine whether the conclusions change using event-specific  $D_{LL}$  rather than the parametric climatological  $D_{LL}$ .

#### 4.1. June 2013

Our first event is a approximately -100 Dst magnetic storm that occurred at the end of May/start of June in 2013. Figure 3 provides an overview of the event. The storm activity was driven by a strongly southward interplanetary magnetic field (IMF), and was accompanied by a gradual increase in solar wind speed (Vsw) from <400 to approximately 800 km. The event, as is common during storms, consisted of a dropout of relativistic electron flux during the main phase, followed by a gradual recovery. We focus our analysis on the 1.1 MeV channel as it is the conventional definition of relativistic electrons and also happens to have nearby MagEIS channels with good counting statistics for computing gradients. We have selected four passes through the belts for further examination, labeled, a, b, c, and d, in panel d. For each pass, we use a sixth-order low-pass Butterworth filter (Butterworth, 1930) to remove fluctuations with periods shorter than 30 min. The filter is applied separately to the natural logarithm of fluxes in each energy channel and pitch angle bin. According to the drift periods in Figure 2, the 30-min low-passed filtered log flux approximates a drift average  $\ln j(p, \alpha, \vec{r}(t))$  throughout the outer zone. This approach neglects the spacecraft motion over the averaging window and obtains a drift average by assuming all particles on the drift shell pass by the spacecraft. Within these assumptions, this approach works even though we are not (yet) using drift-invariant parameters: for a static field, all particles with a given set of invariants will pass through  $\vec{r}(t)$  with the corresponding local pitch angle  $\alpha$  (momentum p does not change in a drift under magnetic-forces only). The detrended residual  $\ln j(p,\alpha,\vec{r}(t)) - \ln j(p,\alpha,\vec{r}(t))$  is, therefore, approximately the drift phase structure. (We perform our mathematical manipulations in natural log, but we will follow the established convention of graphing common log fluxes, i.e.,  $\log_{10} j$ .)

Poisson counting noise could produce apparent drift phase structure. In the plots like panel a.ii of Figure 4, we draw dashed gray lines to indicate the total drift phase amplitude,  $\sqrt{(\Delta \ln j)^2 + C^{-1}}$ , where *C* represents the number of counts in the flux accumulation. Because we have chosen intervals where the flux is adequate to have minimal Poisson noise, these additional curves are not discernible in the plots, except occasionally at the start and end of a plot, because Poisson noise is usually negligible.

We consider in detail the drift structures observed during a few passes of the satellite throughout the storm. The first pass, a, is of interest because it had a large, impulsive drift phase structure, extending down to  $L \sim 3$ , before

O'BRIEN ET AL. 7 of 19

21699402, 2022, 8, Downloaded from https://agupubs.onlinelibrary.wiley.com/doi/10.1029/2021/A030331 by University Of Athens, Wiley Online Library on [29/11/2023]. See the Terms and Conditions (https://onlinelibrary.wiley.

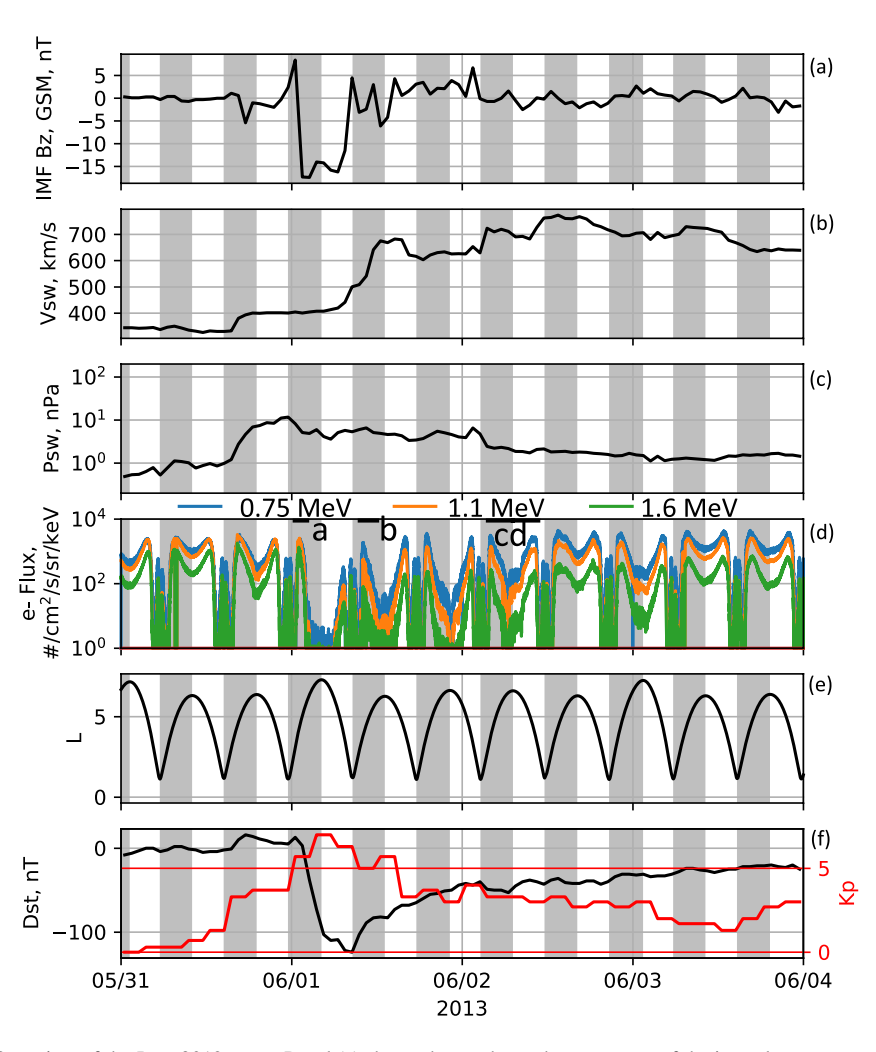


Figure 3. Overview of the June 2013 event. Panel (a) shows the north-south component of the interplanetary magnetic field (the z component in the geocentric, solar magnetospheric coordinate system). Panel (b) shows the solar wind speed. Panel (c) shows the solar wind dynamic pressure. Panel (d) shows locally mirroring flux for the four MagEIS electron channels and also contains horizontal black bars marking the four passes that will be studied in detail. Panel (e) provides the McIlwain L value (Olson-Pfitzer Quiet field model) of the RBSP-B spacecraft. Panel (f) shows the Dst index on the left axis and the Kp index on the right axis. In all panels, gray shading indicates that RBSP is outbound (dL/dt > 0).

the dropout. The other passes plotted occur in the middle of a flux increase. Figure 4 panels a.i, a.ii, and a.iii show pass a in detail. Panel a.i gives the residual drift phase structure in three energy channels near 1 MeV. The impulse and accompanying drift echoes are evident in the first approximately 30 min of the plot. A region of " $\Delta$ L Exclusion" (the horizontal black bar on the border between panels a.i and a.ii) indicates where the change in L over a drift period for a 1 MeV electron is either less than 0.05 or greater than 0.5—in the marked region, the calculation of  $\frac{\partial \ln \overline{f_0}}{\partial L}$  is potentially suspect. Panel a.ii shows the detrended flux in the 1.1 MeV main and histogram channel as well as the detrended total magnetic field (|B|). As with log flux, the detrended |B| is the residual after subtracting a 30-min Butterworth low-pass filtered |B|. The gray shading indicates  $\pm \Delta \ln j$  from Equation 15 converted to common log. For  $D_{LL}$  in Equation 15, we evaluate the climatological Kp-dependent Ozeke et al. (2014) model, which accounts for only electromagnetic perturbations (total electromagnetic ULF wave power). We see that drift phase structure in the fluxes initially follows fluctuations in |B|, but then decouples after approximately 1:00.

Finally, panel a.iii of Figure 4 shows flux versus McIlwain L, where L is obtained from the OPQ model for a locally mirroring particle. Three passes are shown, with the orange pass being the one shown in panels a.i and a.ii. The dark blue pass precedes the orange pass, and the light blue pass follows. Gray shading provides the expected amplitude of drift-phase-structure, derived from the smoothed flux and  $\pm \Delta \ln j$  from Equation 15 for the orange

O'BRIEN ET AL. 8 of 19

21699402, 2022, 8, Downloaded from https://agupubs.onlinelibrary.wiley.com/doi/10.1029/2021/A030331 by University Of Athens, Wiley Online Library on [29/11/2023]. See the Terms and Conditions (https://onlinelibrary.wiley.com/en/rmz

conditions) on Wiley Online Library for rules of use; OA articles

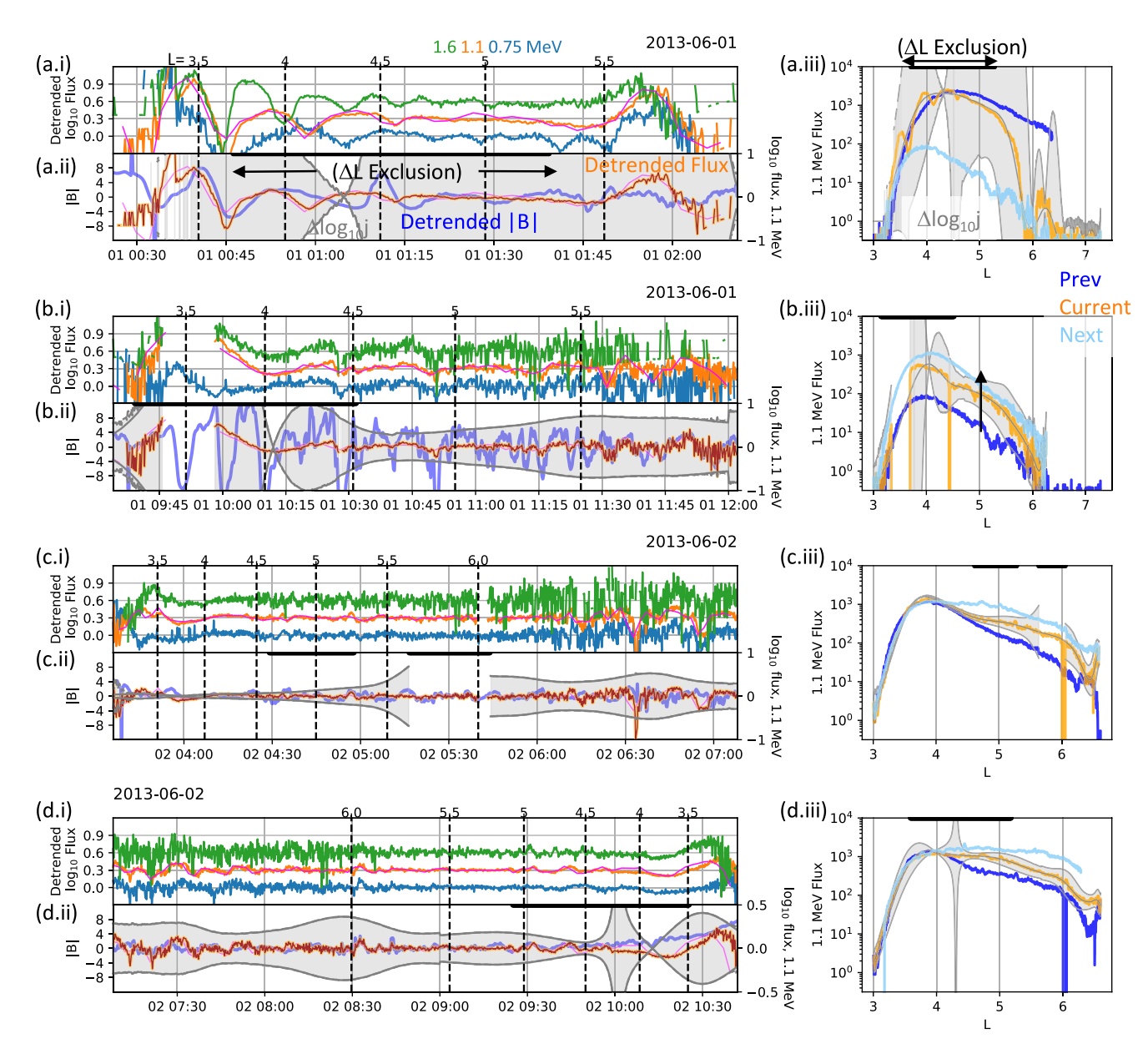
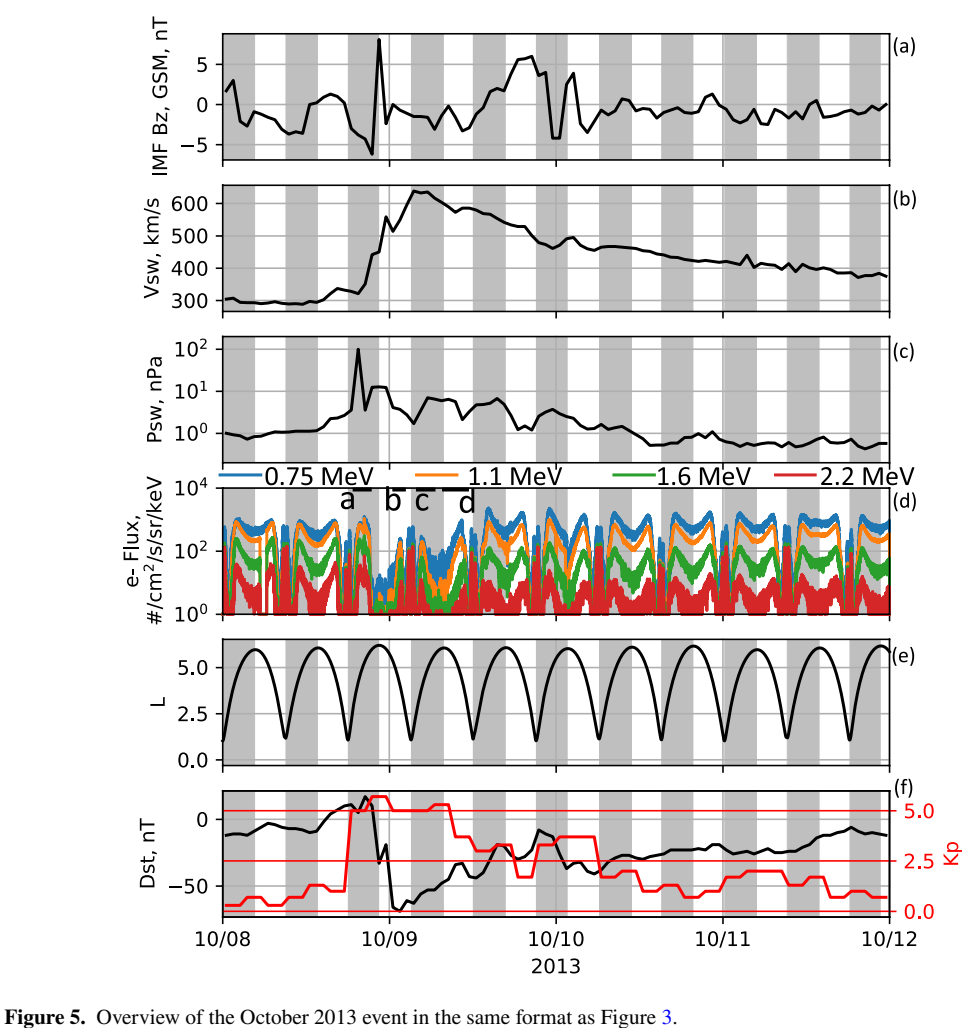


Figure 4. Four selected passes from the June 2013 event. Panel (a.i) shows the detrended  $\log_{10}$  locally mirroring flux in the three MagEIS main channels (arbitrary units, vertically offset). The 1.1 MeV main channel is shown in orange, while a narrow-band histogram channel near the same energy is shown in magenta. Spacecraft L values are indicated. Panel (a.ii) shows the detrended magnetic field strength at RBSP-B (blue, left axis) and the detrended 1.1 MeV  $\log_{10}$  locally mirroring flux (orange and magenta, right axis). Again, orange and magenta refer to the main and histogram channels. Gray shading indicates the  $\pm \Delta \ln j$  boundaries. Panel (a.iii) shows three passes of 1.1 MeV MagEIS locally mirroring flux. The orange trace indicates observed 1.1 MeV flux the same pass shown panels a.i and a.ii. The dark blue shows that pass prior, and light blue shows the following pass. Gray shading indicates the  $\pm \Delta \ln j$  boundaries. The black horizontal bars in (a.ii) and (a.iii) indicate where the change in L over one drift period is either less than 0.05 or greater than 0.5. Panels (b.i) through (d.ii) follow the same format as (a.i) through (a.iii), but present the other three passes noted in Figure 3.

pass. We can see in panels a.ii and a.iii that the large impulse between L=3 and four is not actually large enough to produce radial transport in excess of what is indicated by quasilinear theory and the model  $D_{LL}$ . This is a theme we will see throughout our survey of the three events: the drift phase structure rarely extends outside the  $\pm \Delta \ln j$  range indicated by quasilinear theory. In this particular case, any flux enhancement caused by the impulse is quickly depleted by other main phase loss processes: the light blue trace in panel a.iii is nearly two orders of magnitude down from the orange trace, indicating a sharp drop in flux over approximately 4 hr.

O'BRIEN ET AL. 9 of 19

21699402, 2022, 8, Downloaded from https://agupubs.onlinelibrary.wiley.com/doi/10.1029/2022/A030331 by University Of Athens, Wiley Online Library on [29/11/2023]. See the Terms and Conditions (https://onlinelibrary.onlinelibra



While pass a was chosen because of its large, obvious impulse, we chose passes b-d because they occur while the flux is increasing across all L shells. Panels b-d in Figure 4 are in the same format as their counterparts in panel a. In all three passes b-d, the orange and magenta traces, which represent the detrended flux, almost never reach outside the gray shaded region. This indicates that, although the flux is increasing, the drift phase structure is too small to indicate significant nonquasilinear radial transport. We note that the 1.6 MeV (green) channel is experiencing substantial Poisson noise during this and several of the later intervals under study.

The 1.1 MeV main and histogram channel shown in Figure 4 both have a center energy of 1,064 keV. The main channel's energy bandwidth is 309 keV FWHM (29%). The histogram channel's energy bandwidth is 96 keV (9%). Yet the two channels show very similar drift phase structure. The histogram channel does not show larger amplitude or qualitatively different structure, and so it is unlikely that significant structure is being hidden by the width of the main channel. We will see this behavior repeated in the other two events we will examine.

#### 4.2. October 2013

The next event we have chosen to study occurred in early October 2013, as shown in Figure 5. A modest sized storm occurs on October 8th and ninth and recovers over several days. The storm is accompanied by modest southward IMF and a rapid increase in solar wind speed. Again, the relativistic electron flux drops out during the main phase and recovers over the following days. We have selected four passes, labeled a, b, c, and d in panel d, from the main phase and early recovery phase for detailed examination.

O'BRIEN ET AL. 10 of 19

21699402, 2022. 8, Downloaded from https://agupubs.onlinelibrary.wiley.com/doi/10.1029/2022/A030331 by University Of Athens, Wiley Online Library on [29/11/2023]. See the Terms and Conditions (https://onlinelibrary.wiley.com/error

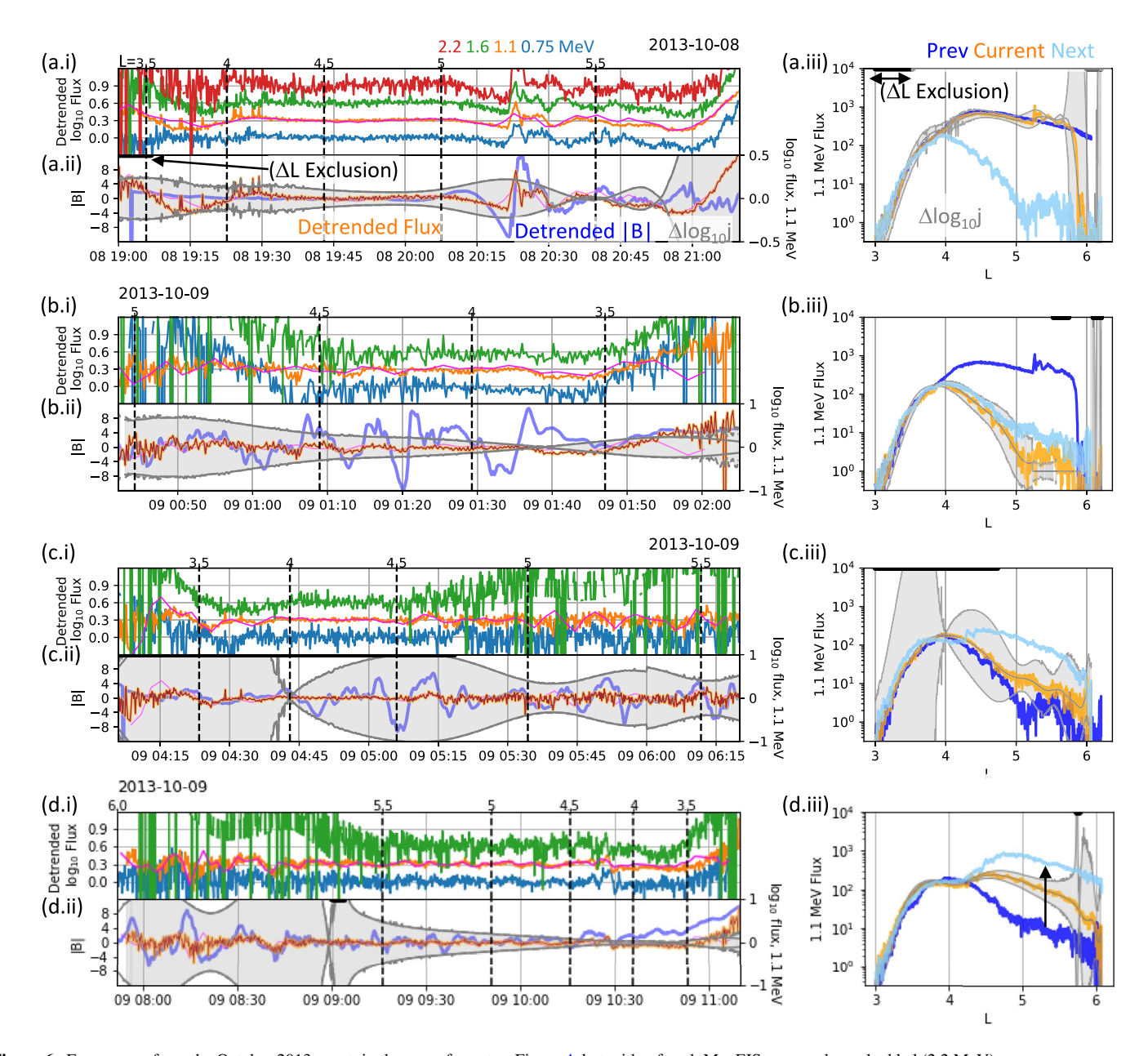


Figure 6. Four passes from the October 2013 event, in the same format as Figure 4, but with a fourth MagEIS energy channel added (2.2 MeV).

Pass a is shown in Figure 6 panels a.i, a.ii, and a.iii, following the same format as Figure 4. We chose pass a because of the small impulse observed near  $L \sim 5$  around 20:00 on October 8th. This impulse produced some drift echoes, as can be seen in panel a.i. Panel a.ii shows that the impulse also caused the residual flux to briefly extend outside the  $\pm \Delta \ln j$  boundary around 20:20. The associated impulse in |B| indicates that this is an electromagnetic impulse causing rapid radial transport that is stronger than indicated by the quasilinear model. However, panel a.iii shows that as with the impulse in Figure 4, the flux actually goes down significantly in the hours after the impulse, on account of main phase loss processes.

Pass b, shown in Figure 6 panels b.i, b.ii, and b.iii, exhibits ongoing drift phase structure that is correlated with fluctuations in the magnetic field. However, the drift phase structure is smaller than what would be required to produce more transport than indicated by the quasilinear  $D_{LL}$ . Nonetheless, as shown in panel b.iii, flux is increasing at all L values in the outer zone. Passes c and d, shown in panels c.i through d.iii show weak drift phase structure, far smaller than  $\pm \Delta \ln j$  from  $D_{LL}$ . Panel d.i and d.ii show a very clear case of drift relatively weak drift phase structure while the fluxes are increasing over the range L > 4.5. Panel d.ii also shows something we see

O'BRIEN ET AL.

21699402, 2022, 8, Downloaded from https://agupubs.onlinelibrary.wiley.com/doi/10.1029/2021A030331 by University Of Athens, Wiley Online Library on [29/11/2023]. See the Terms and Conditions (https://onlinelibrary.onlinelibrary.wiley.com/doi/10.1029/2021A030331 by University Of Athens, Wiley Online Library on [29/11/2023]. See the Terms and Conditions (https://onlinelibrary.onlinelibrary.wiley.com/doi/10.1029/2021A030331 by University Of Athens, Wiley Online Library.on [29/11/2023]. See the Terms and Conditions (https://onlinelibrary.onlinelibrary.wiley.com/doi/10.1029/2021A030331 by University Of Athens, Wiley Online Library.on [29/11/2023]. See the Terms and Conditions (https://onlinelibrary.onlinelibrary

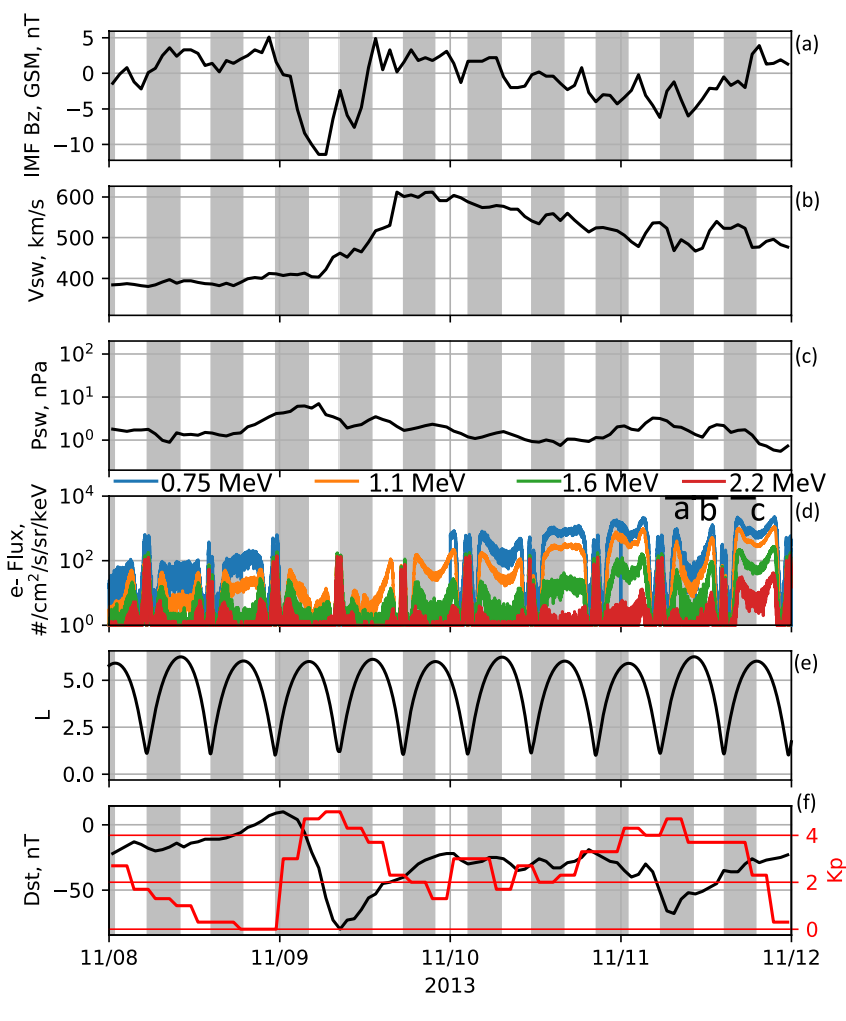


Figure 7. Overview of the November 2013 event in the same format as Figure 3.

in a number of passes: as we approach a steep L gradient in the flux, the residual of the 30-min smoothed flux sometimes curves upward or downward and can extend outside the gray shading for  $\pm \Delta \ln j$ . We interpret these as edge effects on the residual flux calculation, since they are one-sided (i.e., the flux only goes up or down, it does not vary in both directions).

#### 4.3. November 2013

The final event we examine occurred in early November 2013, shown in Figure 7. The event consists of two main phases with Dst < -50 nT. The first one is accompanied by stronger southward IMF and is accompanied by a gradual increase in solar wind speed from approximately 400 to 600 km/s. The second main phase is smaller and is accompanied by weaker southward IMF. We examined all passes during the entire 4-day interval shown in Figure 7, and selected three from the second Dst recovery for more detailed study. These three passes are labeled a, b, and c, in panel d.

Figure 8 shows the three selected passes in detail. Panels a.i, a.ii, and a.iii provide details of pass a. Panel a.ii shows some drift phase structure that is correlated with fluctuations in the magnetic field. This drift phase structure is partially reflected in the (noisy) 0.75 and 1.6 MeV channels, suggesting that it is field line motion causing the drift phase structure. However, for the most part, this structure is never large enough to extend outside the gray  $\pm \Delta \ln j$  boundaries. Panel a.iii shows that this pass is associated with a drop in the electron flux across the entire outer zone. The next pass, b, is shown in panels b.i, b.ii, and b.iii. Panels b.i and b.ii show that this pass is relatively free of drift phase structure. The  $\pm \Delta \ln j$  boundaries are fairly narrow in b.ii and b.iii, and yet the flux

O'BRIEN ET AL. 12 of 19

21699402, 2022, 8, Downloaded from https://agupubs.onlinelibrary.wiley.com/doi/10.1029/2022/A030331 by University Of Athens, Wiley Online Library on [29/11/2023]. See the Terms and Condit

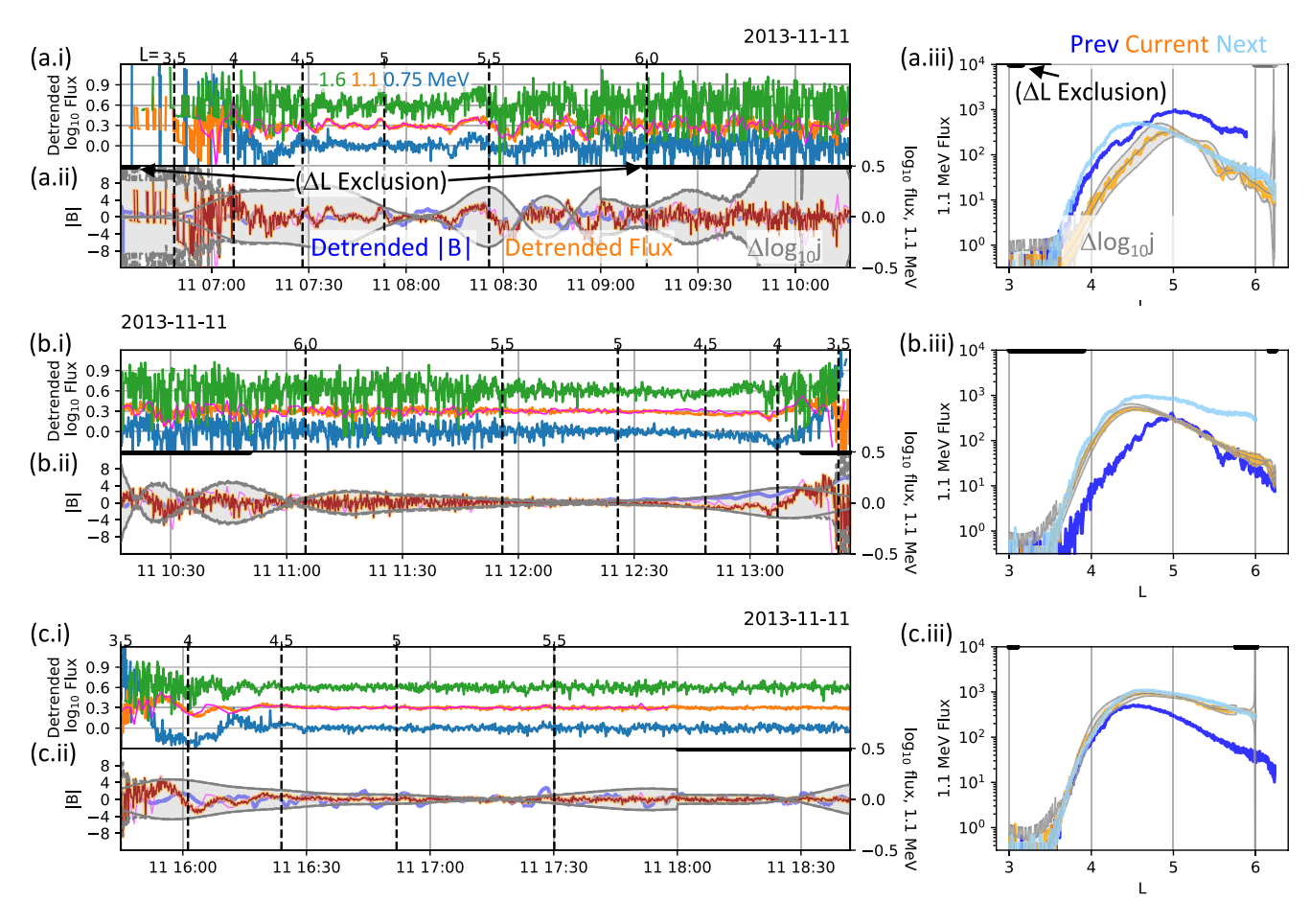


Figure 8. Three passes from the November 2013 event, in the same format as Figure 4.

does not extend outside them much. Where the flux does extend outside the boundaries, it appears to be Poisson fluctuations, rather than genuine drift phase structure. The final pass, c, is shown in panels c.i through c.iii. Below  $L \sim 4.5$  there is some drift phase structure, but it stays within the  $\pm \Delta \ln j$  boundaries. After crossing  $L \sim 4.5$ , the  $\pm \Delta \ln j$  boundaries are again fairly narrow, but the drift phase structure is also very narrow. Again, the drift phase structure does not extend outside the boundaries, suggesting whatever radial transport is occurring during these passes is dominated by quasilinear  $D_{LL}$ .

#### 4.4. June 2013—With Event-Specific $D_{II}$

Up to this point, we have used a climatological Kp-driven  $D_{LL}$ , from Ozeke et al. (2014). However, because there is considerable variation in  $D_{LL}$  around these climatological models (Sandhu et al., 2021), it is better to use event-specific  $D_{LL}$ . It is possible, with some effort, to produce event-specific  $D_{LL}$  to use in Equation 15, and we have done so for the first event, May–June 2013. Figure 9 shows the first two passes from Figures 3 and 4. Panels a.i through a.iii are repeated from Figure 3. Panel a.iv shows the climatological  $D_{LL}$  and the event-specific  $D_{LL}$ . We see that the prior to 01:11, the event-specific  $D_{LL}$  is smaller than the climatological  $D_{LL}$ , leading to narrow  $\pm \Delta \ln j$  boundaries (compare gray shading between panels a.ii and a.v). In this interval, the (electro)magnetic fluctuations cause drift phase structures that do briefly extend outside the gray  $\pm \Delta \ln j$  boundaries around  $L \sim 3.5$ . However, from 01:11 onward, the drift phase structure remains within the  $\pm \Delta \ln j$  boundaries, suggesting a return to the quasilinear radial transport regime. As noted above, any flux enhancement caused by this magnetic impulse is ultimately lost subsequently during the storm main phase, as the flux drops by several orders of magnitude before the next pass through the belts (panels a.iii and a.vi).

O'BRIEN ET AL. 13 of 19

21699402, 2022. 8, Downloaded from https://agupubs.onlinelibrary.wiley.com/doi/10.1029/2022JA030331 by University Of Athens, Wiley Online Library on [29/11/2023]. See the Terms and Conditions (https://onlinelibrary.wiley.com/terms-

emed by the applicable Creative Commons Licens

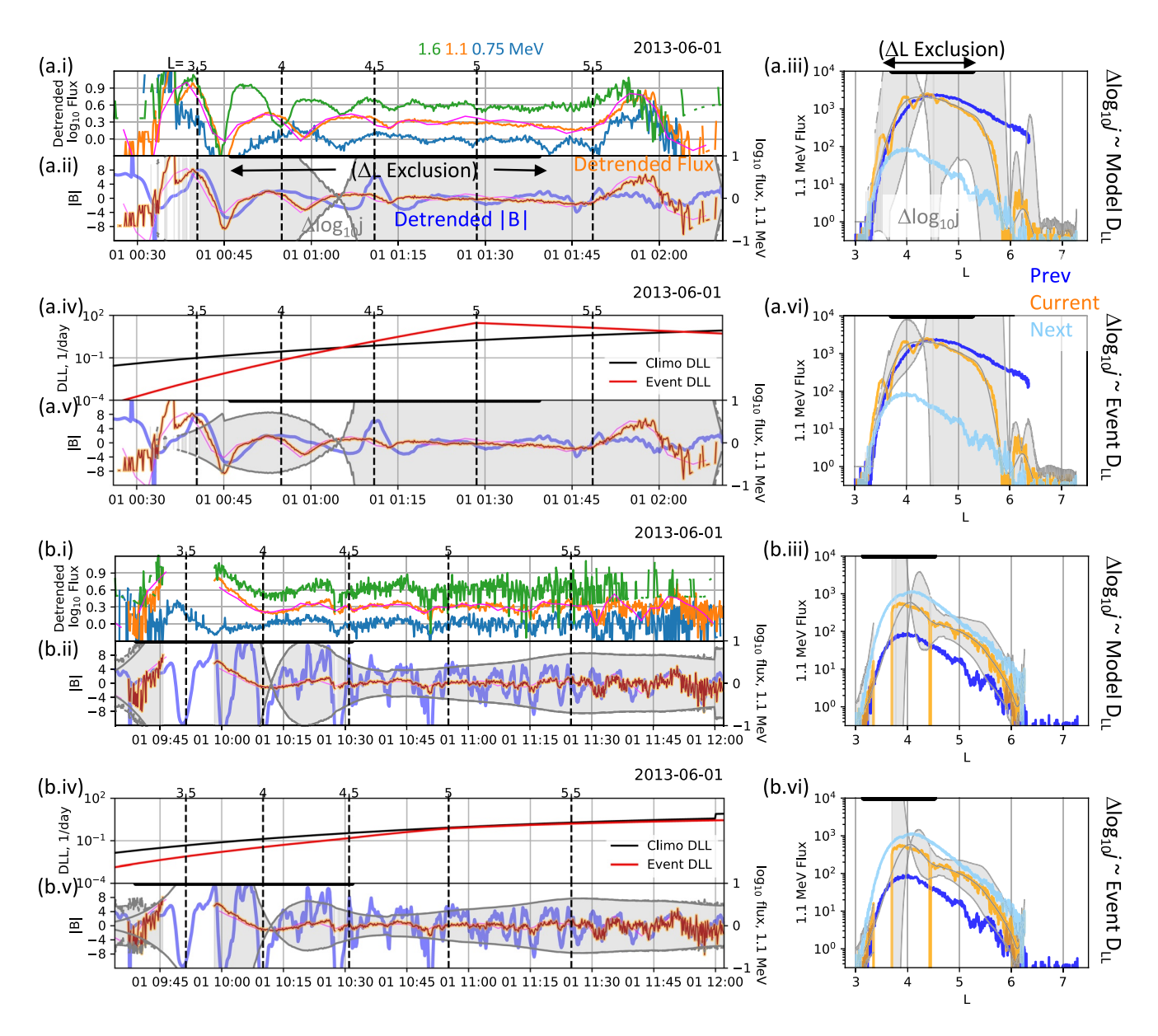


Figure 9. Four selected passes from the June 2013 event. Panels (a.i-a.iii) are repeated from Figure 4, showing pass a from 3. Panel (a.iv) compares  $D_{LL}$  for the Ozeke et al. (2014) climatological model to the event-specific  $D_{LL}$ . Panels (a.v) and (a.vi) follow the same format as panels (a.ii) and (a.iii), except using the event-specific  $D_{LL}$  to compute the  $\pm \Delta \ln j$  boundaries. Panels (b.i-b.vi) follow the same pattern, showing pass b from Figure 3.

Panels b.i through b.vi in Figure 9 show pass b from Figures 3 and 4. Again, the event-specific  $D_{LL}$  is smaller than the climatological  $D_{LL}$  up to about  $L \sim 5$ , as shown in panel b.iv. However, in this pass, the drift phase structures in panel b.v do not extend outside the  $\pm \Delta \ln j$  boundaries. Thus, even the somewhat narrower boundaries implied by the weaker  $D_{LL}$  do not cause us to reject the hypothesis that radial transport is largely quasilinear.

We examined the other passes shown in Figures 3 and 4, which showed event-specific  $D_{LL}$  larger than the climatological model. Thus, those passes also leave the null hypothesis intact.

O'BRIEN ET AL. 14 of 19

### 5. Discussion and Conclusion

Starting with a null hypothesis that radial transport is mainly caused by quasilinear diffusion, we tested that hypothesis against observed drift phase structure across three events. In these three events, the drift phase structure generally does not exceed the amplitudes implied by quasilinear diffusion. This is true whether we use a climatological model of  $D_{IL}$  or event-specific  $D_{IL}$ .

When drift phase structure occurs that is larger than the quasilinear expectation, it is associated with (electro-)magnetic impulses (see, e.g., Figure 6 panel a.ii and Figure 9 panel a.v.). Although it is clearly possible for magnetic impulses to result in radial transport (famously in the March 1991 event; Li et al., 1993), in the examples we studied, any belt enhancement caused by the transport event was subsequently lost during the main phase of the storm. This seems a likely fate of many impulses driven by storm sudden commencements—the initial pressure pulse may drive dramatic inward radial transport, only to have the transported particles lost during the main phase of the ensuing storm. We suggest that if the impulse is large enough, and the subsequent storm is not too large, an initially transported population may survive the main phase, as happened in March 1991 and other shock events.

In the events we studied, there is very little storm-time drift phase structure observed at approximately 1 MeV, and what structure is there is not strongly correlated with flux increases. This is entirely consistent with quasilinear radial diffusion—interaction of electrons with broad-band, random-phase ULF power. Formally, we accept the null hypothesis of quasilinear radial diffusion being the primary cause of radial transport. However, there are some limitations to our analysis that are worth discussing.

First, we have worked entirely in fluxes, and have not accounted for the Dst effect (Dessler & Karplus, 1961). This effect can lead to decreases or increases in the electron flux through slow changes in the global magnetic field topology without changing the  $L^*$  invariant of the electrons. Passes c and d of the June 2013 event (Figures 3 and 4) are at approximately the same Dst; both are in the middle of flux increases, suggesting that, if the increase is due in part to radial transport, it is achieved via quasilinear diffusion.

Second, we have based our analysis on  $D_{LL}$  computed from spatially limited observations of the electromagnetic fields. To convert those fields to  $D_{LL}$  requires some assumptions about the spatial structure of those fields. It is possible, then, that some as-yet-unidentified deficiency exists in the inferred  $D_{LL}$ , causing it to be too large. For example, the azimuthal mode number m of the ULF waves is typically unknown and assumed to be 1. However, Ozeke et al. (2014) explored the effects of assuming m=10 instead of m=1 and found this often reduced  $D_{LL}$  by around a factor of 2–3. Still, if for some reason the quasilinear  $D_{LL}$  is too large, then we are overestimating the corresponding  $\pm \Delta \ln j$ .

Third, our finite sensor resolution may be masking hidden drift phase structure. The absence of observed drift phase structure arises from drift phase mixing. At a fine scale, this drift phase mixing never truly disappears. It only disappears in practice because our sensors cannot resolve the finest scales. Therefore, in the absence of other processes, it is almost a certainty that with sufficiently fine sensor resolution, there will be drift phase structure. However, we investigated this with the MagEIS histogram channel data and did not find a dramatic effect.

Our analysis, then, leaves something of a conundrum. Some test particle simulations have argued that the quasilinear diffusion limit is only achieved when aggregating over many storms (Chen et al., 1992; Riley & Wolf, 1992; Ukhorskiy et al., 2006; Ukhorskiy & Sitnov, 2008, 2012). For reasons that are not yet clear, the observations contradict those simulations. Notably, the earlier papers left open the possibility that at higher energies (e.g., above 130 keV at  $L \sim 3$ ) radial diffusion might be appropriate. Because the real magnetosphere also involves processes that violate the first and second adiabatic invariants, it is also possible that this fine drift phase structure is truly washed out. As noted by Sorathia et al. (2018), these sophisticated radial transport models, those that involve test particle tracing in magnetohydrodynamic (MHD) fields, do not yet include processes that violate the first and second adiabatic invariants. Such processes will mix particles together as they move radially, often involving diffusion in the first and second adiabatic invariants, and sometimes also the third (e.g., O'Brien, 2015). Gyroresonant wave-particle interactions will act on the energy and pitch-angle gradients created by drift phase structure, eroding that structure more rapidly in direct proportion to the steepness of the gradients, and intermingling particles on different radial transport trajectories. As the community develops models capable of including gyroresonant processes and test particle transport in MHD fields, we expect to gain insight whether

O'BRIEN ET AL. 15 of 19

gyroresonant process contribute to a more quasilinear radial transport outcome on a storm-by-storm basis, or whether there is some other explanation for why there is less drift phase structure in the data than would be expected from the simulations.

# **Appendix A: Estimation of PSD Gradient From Flux**

In this Appendix, we will provide the necessary steps to compute  $\frac{\partial \ln \overline{f}_0}{\partial L}\Big|_{M,K}$  from flux observed as a function of momentum p, local pitch angel  $\alpha$ , and position  $\vec{r}$  along a spacecraft orbit. First, we recognize that the position along the spacecraft trajectory can be replaced with time t:

$$j(p,\alpha,t) = j(p,\alpha,\vec{r}(t)) \tag{A1}$$

Next, we consider the time average of  $\ln j$ :

$$\overline{\ln j}(p,\alpha,t) \approx \left\langle \ln j \left( p,\alpha,\vec{r}(t) \right) \right\rangle_{\tau_d} \approx 2 \ln p + \left\langle \ln f \left( M,K,L,\phi_3 \right) \right\rangle_d \tag{A2}$$

Before the impulse, then, we have:

$$\overline{\ln j_0}(p,\alpha,t) \approx 2 \ln p + \ln \overline{f_0}(M(p,\alpha,t), K(\alpha,t), L(\alpha,t)) \tag{A3}$$

Taking the three derivatives of  $\overline{\ln j_0}$ , we have:

$$\frac{\partial \overline{\ln j_0}}{\partial \ln p}\Big|_{\alpha,t} \approx 2 + \frac{\partial \overline{\ln f_0}}{\partial \ln M}\Big|_{K,L} \frac{\partial \overline{\ln M}}{\partial \ln p}\Big|_{\alpha,t} \tag{A4}$$

$$\frac{\partial \overline{\ln j_0}}{\partial \alpha}\Big|_{p,l} \approx \frac{\partial \overline{\ln f_0}}{\partial \overline{\ln M}}\Big|_{K,L} \frac{\partial \overline{\ln M}}{\partial \alpha}\Big|_{p,l} + \frac{\partial \overline{\ln f_0}}{\partial K}\Big|_{M,L} \frac{\partial K}{\partial \alpha}\Big|_{p,l} + \frac{\partial \overline{\ln f_0}}{\partial L}\Big|_{M,K} \frac{\partial L}{\partial \alpha}\Big|_{p,l}$$
(A5)

$$\frac{\partial \overline{\ln j_0}}{\partial t}\Big|_{p,\alpha} \approx \frac{\partial \overline{\ln f_0}}{\partial \overline{\ln M}}\Big|_{K,L} \frac{\partial \overline{\ln M}}{\partial t}\Big|_{p,\alpha} + \frac{\partial \overline{\ln f_0}}{\partial K}\Big|_{M,L} \frac{\partial K}{\partial t}\Big|_{p,\alpha} + \frac{\partial \overline{\ln f_0}}{\partial L}\Big|_{M,K} \frac{\partial L}{\partial t}\Big|_{p,\alpha}$$
(A6)

This gives us a system of three Equations A4–A6 in three unknowns:  $\frac{\partial \ln \overline{f_0}}{\partial \ln M}$ ,  $\frac{\partial \ln \overline{f_0}}{\partial K}$ , and  $\frac{\partial \ln \overline{f_0}}{\partial L}$ , with the last being the quantity we desire. The derivatives  $\frac{\partial \ln \overline{f_0}}{\partial \ln p}$ ,  $\frac{\partial \ln \overline{f_0}}{\partial a}$ , and  $\frac{\partial \ln \overline{f_0}}{\partial t}$  are taken numerically from the low-pass-filtered flux observations. The partial derivatives  $\frac{\partial \ln M}{\partial \ln p}\Big|_{a,t}$  and  $\frac{\partial \ln M}{\partial a}\Big|_{p,t}$  can be obtained analytically from Equation 2:

$$\frac{\partial \ln M}{\partial \ln p}\Big|_{\alpha,l} = 2\tag{A7}$$

$$\frac{\partial \ln M}{\partial \alpha}\Big|_{n,t} = \frac{2}{\tan \alpha} \tag{A8}$$

The derivative  $\frac{\partial \ln M}{\partial t}$  depends only on B(t) along the spacecraft track:

$$\frac{\partial \ln M}{\partial t}\Big|_{\alpha,t} = -\frac{d \ln B}{dt} \tag{A9}$$

The remaining derivatives  $\frac{d \ln B}{dt}$ ,  $\frac{\partial K}{\partial \alpha}$ ,  $\frac{\partial L}{\partial \alpha}$ ,  $\frac{\partial K}{\partial t}$ , and  $\frac{\partial L}{\partial t}$  can be obtained numerically from the TS04D magnetic ephemeris files provided by the Radiation Belt Storm Probes Energetic Particle, Composition, and Thermal Plasma (RBSP-ECT) science operations center (Spence et al., 2013). We can, therefore, rewrite (A4)-(A6) as a matrix-vector problem:

$$\begin{pmatrix}
\frac{\partial \overline{\ln j_0}}{\partial \ln p} \Big|_{\alpha,t} - 2 \\
\frac{\partial \overline{\ln j_0}}{\partial \alpha} \Big|_{p,t} \\
\frac{\partial \overline{\ln j_0}}{\partial t} \Big|_{p,\alpha}
\end{pmatrix} \approx \begin{pmatrix}
\frac{\partial \ln M}{\partial \ln p} \Big|_{\alpha,t} & 0 & 0 \\
\frac{\partial \ln M}{\partial \alpha} \Big|_{p,t} & \frac{\partial K}{\partial \alpha} \Big|_{p,t} & \frac{\partial L}{\partial \alpha} \Big|_{p,t} \\
\frac{\partial \ln J_0}{\partial t} \Big|_{p,\alpha} & \frac{\partial K}{\partial t} \Big|_{p,\alpha} & \frac{\partial L}{\partial t} \Big|_{p,\alpha}
\end{pmatrix} \begin{pmatrix}
\frac{\partial \ln \overline{j_0}}{\partial \ln M} \Big|_{K,L} \\
\frac{\partial \ln \overline{j_0}}{\partial K} \Big|_{M,L} \\
\frac{\partial \ln \overline{j_0}}{\partial L} \Big|_{M,K}
\end{pmatrix} (A10)$$

O'BRIEN ET AL. 16 of 19

21699402, 2022, 8, Downloaded from https://agupubs

1029/2022JA030331 by University Of Athens,

Wiley Online Library on [29/11/2023]. See,

Solving this matrix-vector problem yields  $\frac{\partial \ln \overline{f}_0}{\partial L}\Big|_{M,K}$  as well as  $\frac{\partial \ln \overline{f}_0}{\partial \ln M}\Big|_{K,L}$  and  $\frac{\partial \ln \overline{f}_0}{\partial K}\Big|_{M,L}$ .

We note that Equation A10 is essentially a coordinate transform from a  $(p, \alpha, t)$  system to an (M, K, L) system, combined with the PSD to flux conversion (the "-2" on the left-hand side). It relates drift-averaged PSD to time-averaged flux. The transform breaks down when the matrix becomes singular. So, in practice, we exclude such singular points from our analysis.

#### **Data Availability Statement**

RRBSP data are available at cdaweb.gsfc.nasa.gov. Omni data are available at omniweb.gsfc.nasa.gov. CARISMA ground magnetometer data can be obtained at www.carisma.ca. Data used in this study can be found at doi: 10.5281/zenodo.5796400.

#### Acknowledgments References

The authors thank I. Mann and A. Boyd for helpful discussions. The authors thank D.K. Milling and the rest of the CARISMA team for data. CARISMA is operated by the University of Alberta, funded by the Canadian Space Agency. This work was supported by NASA LWS grant NNX14AF99G, and by RBSP-ECT funding provided by JHU/APL contract 967399 under NASA's Prime contract

NAS5-01072.

- Ali, A. F., Elkington, S. R., Tu, W., Ozeke, L. G., Chan, A. A., & Friedel, R. H. W. (2015). Magnetic field power spectra and magnetic radial diffusion coefficients using CRRES magnetometer data. *Journal of Geophysical Research: Space Physics*, 120, 973–995. https://doi. org/10.1002/2014JA020419
- Ali, A. F., Malaspina, D. M., Elkington, S. R., Jaynes, A. N., Chan, A. A., Wygant, J., & Kletzing, C. A. (2016). Electric and magnetic radial diffusion coefficients using the Van Allen probes data. *Journal of Geophysical Research: Space Physics*, 121, 9586–9607. https://doi. org/10.1002/2016JA023002
- Blake, J. B., Carranza, P. A., Claudepierre, S. G., Clemmons, J. H., Crain, W. R., Dotan, Y., et al. (2013). The magnetic electron ion spectrometer (MagEIS) instruments aboard the radiation belt storm probes (RBSP) spacecraft. *Space Science Reviews*, 179, 383–421. https://doi.org/10.1007/s11214-013-9991-8
- Boscher, D., Bourdarie, S., & Beutier, T. (1996). Dynamic modeling of trapped particles. *IEEE Transactions on Nuclear Science*, 43(2), 416–425. https://doi.org/10.1109/23.490890
- Brautigam, D. H., & Albert, J. M. (2000). Radial diffusion analysis of outer radiation belt electrons during the October 9, 1990, magnetic storm. Journal of Geophysical Research, 105(A1), 291–309. https://doi.org/10.1029/1999JA900344
- Brautigam, D. H., Ginet, G. P., Albert, J. M., Wygant, J. R., Rowl, D. R., Ling, A., & Bass, J. (2005). CRRES electric field power spectra and radial diffusion coefficients. *Journal of Geophysical Research*, 110, A02214. https://doi.org/10.1029/2004JA010612
- Brewer, H. R., Schulz, M., & Eviatar, A. (1969). Origin of drift-periodic echoes in the outer-zone electron flux. *Journal of Geophysical Research*, 74(1). https://doi.org/10.1029/ja074i001p00159
- Butterworth, S. (1930). On the theory of filter amplifiers. Experimental Wireless & the Wireless Engineer, 7, 536-541.
- Chen, M. W., Schulz, M. S., Lyons, L. R., & Gorney, D. J. (1992). Ion radial diffusion in an electrostatic impulse model for stormtime ring current formation. *Geophysical Research Letters*, 19(6), 621–624. https://doi.org/10.1029/92g100392
- Chen, X.-R., Zong, Q.-G., Zhou, X.-Z., Blake, J. B., Wygant, J. R., & Kletzing, C. A. (2017). Van Allen Probes observation of a 360° phase shift in the flux modulation of injected electrons by ULF waves. Geophysical Research Letters, 44, 1614–1624. https://doi.org/10.1002/2016GL071252
- Claudepierre, S. G., Blake, J. B., Boyd, A. J., Clemmons, J. H., Fennell, J. F., Gabrielse, C., et al. (2021). The magnetic electron Ion Spectrometer: A review of on-orbit sensor performance, data, operations, and Science. *Space Science Reviews*, 217(80), 2021. https://doi.org/10.1007/s11214-021-00855-2
- Claudepierre, S. G., Mann, I. R., Takahashi, K., Fennell, J. F., Hudson, M. K., Blake, J. B., et al. (2013). Van Allen Probes observation of localized drift resonance between poloidal mode ultra-low frequency waves and 60 keV electrons. *Geophysical Research Letters*, 40, 4491–4497. https://doi.org/10.1002/grl.50901
- Cornwall, J. M. (1968). Diffusion processes influenced by conjugate-point wave phenomena. *Radio Science*, 3, 740–744. https://doi.org/10.1002/rds196837740
- Cornwall, J. M. (1972). Radial diffusion of ionized helium and protons: A probe for magnetospheric dynamics. *Journal of Geophysical Research*, 77(10), 1756–1770. https://doi.org/10.1029/JA077i010p01756
- Dessler, A. J., & Karplus, R. (1961). Some effects of diamagnetic ring currents on Van Allen radiation. *Journal of Geophysical Research*, 66(8), 2289–2295. https://doi.org/10.1029/JZ066i008p02289
- Elkington, S. R., Hudson, M. K., & Chan, A. A. (2003). Resonant acceleration and diffusion of outer zone electrons in an asymmetric geomagnetic field. *Journal of Geophysical Research*, 108, 1116. https://doi.org/10.1029/2001JA009202
- Falthammar, C.-G. (1965). Effects of time-dependent electric fields on geomagnetically trapped radiation. *Journal of Geophysical Research*, 70(11) 2503–2516. https://doi.org/10.1009/jet/700011-000503
- 70(11), 2503–2516. https://doi.org/10.1029/jz070i011p02503

  Falthammar, C.-G. (1968). Radial diffusion by violation of the third adiabatic invariant. In B. M. McCormac (Ed.), *Earth's particles and fields* (p. 157). Reinhold Publishing Corp.
- Fei, Y., Chan, A. A., Elkington, S. R., & Wiltberger, M. J. (2006). Radial diffusion and MHD particle simulations of relativistic electron transport by ULF waves in the September 1998 storm. *Journal of Geophysical Research*, 111, A12209. https://doi.org/10.1029/2005JA011211
- Foster, J. C., Wygant, J. R., Hudson, M. K., Boyd, A. J., Baker, D. N., Erickson, P. J., & Spence, H. E. (2015). Shock-induced prompt relativistic electron acceleration in the inner magnetosphere. *Journal of Geophysical Research: Space Physics*, 120, 1661–1674. https://doi.org/10.1002/2014JA020642
- Glauert, S. A., Horne, R. B., & Meredith, N. P. (2014). Three-dimensional electron radiation belt simulations using the BAS Radiation Belt Model with new diffusion models for chorus, plasmaspheric hiss, and lightning-generated whistlers. *Journal of Geophysical Research: Space Physics*, 119, 268–289. https://doi.org/10.1002/2013JA019281
- Hao, Y. X., Zhao, X. X., Zong, Q.-G., Zhou, X.-Z., Rankin, R., Chen, X. R., et al. (2020). Simultaneous observations of localized and global drift resonance. *Geophysical Research Letters*, 47, e2020GL088019. https://doi.org/10.1029/2020GL088019

O'BRIEN ET AL. 17 of 19



# Journal of Geophysical Research: Space Physics

- 10.1029/2022JA030331
- Hao, Y. X., Zong, Q.-G., Zhou, X.-Z., Rankin, R., Chen, X. R., Liu, Y., et al. (2019). Global-scale ULF waves associated with SSC accelerate magnetospheric ultrarelativistic electrons. *Journal of Geophysical Research: Space Physics*, 124, 1525–1538. https://doi.org/10.1029/2018JA026134
- Hartinger, M. D., Claudepierre, S. G., Turner, D. L., Reeves, G. D., Breneman, A., Mann, I. R., et al. (2018). Diagnosis of ULF wave-particle interactions with megaelectron volt electrons: The importance of ultrahigh-resolution energy channels. *Geophysical Research Letters*, 45, 10883–10892. https://doi.org/10.1029/2018GL080291
- Hartinger, M. D., Reeves, G. D., Boyd, A., Henderson, M. G., Turner, D. L., Komar, C. M., et al. (2020). Why are there so few reports of high-energy electron drift resonances? Role of radial phase space density gradients. *Journal of Geophysical Research: Space Physics*, 125, e2020JA027924. https://doi.org/10.1029/2020JA027924
- Huang, C.-L., Spence, H. E., Hudson, M. K., & Elkington, S. R. (2010). Modeling radiation belt radial diffusion in ULF wave fields: 2. Estimating rates of radial diffusion using combined MHD and particle codes. *Journal of Geophysical Research*, 115, A06216. https://doi.org/10.1029/2009JA014918
- Hudson, M., Jaynes, A., Kress, B., Li, Z., Patel, M., Shen, X., et al. (2017). Simulated prompt acceleration of multi-MeV electrons by the 17 March 2015 interplanetary shock. *Journal of Geophysical Research: Space Physics*, 122, 10. https://doi.org/10.1002/2017ja024445
- Hudson, M. K., Elkington, S. R., Li, Z., Patel, M., & Patel, M. (2020). Drift echoes and flux oscillations: A signature of prompt and diffusive changes in the radiation belts. *Journal of Atmospheric and Solar-Terrestrial Physics*, 207, 105332. https://doi.org/10.1016/j.jastp.2020.105332
- Jaynes, A. N., Ali, A. F., Elkington, S. R., Malaspina, D. M., Baker, D. N., Li, X., et al. (2018). Fast diffusion of ultrarelativistic electrons in the outer radiation belt: 17 March 2015 storm event. Geophysical Research Letters, 45, 10874–10882. https://doi.org/10.1029/2018gl079786
- King, J. H., & Papitashvili, N. E. (2005). Solar wind spatial scales in and comparisons of hourly Wind and ACE plasma and magnetic field data. Journal of Geophysical Research, 110(A2), A02209. https://doi.org/10.1029/2004JA010649
- Kletzing, C., Kurth, W. S., Acuna, M., MacDowall, R. J., Torbert, R. B., Averkamp, T., et al. (2013). The electric and magnetic field instrument suite and integrated science (EMFISIS) on RBSP. Space Science Reviews, 179, 127–181. https://doi.org/10.1007/s11214-013-9993-6
- Kokubun, S., Kivelson, M. G., McPherron, R. L., & Russell, C. T. (1977). OGO 5 observations of Pc 5 waves: Particle flux modulations. *Journal of Geophysical Research*, 82(19), 2744–2786. https://doi.org/10.1029/ja082i019p02774
- Kress, B. T., Hudson, M. K., Looper, M. D., Albert, J., Lyon, J. G., & Goodrich, C. C. (2007). Global MHD test particle simulations of >10 MeV radiation belt electrons during storm sudden commencement. *Journal of Geophysical Research*, 112, A09215. https://doi. org/10.1029/2006JA012218
- Lanzerotti, L., & Wolfe, A. (1980). Particle diffusion in the geomagnetosphere: Comparison of estimates from measurements of magnetic and electric field fluctuations. *Journal of Geophysical Research*, 85(A5), 2346–2348. https://doi.org/10.1029/JA085iA05p02346
- Lanzerotti, L. J., Maclennan, C. G., & Schulz, M. (1970). Radial diffusion of outer-zone electrons: An empirical approach to third-invariant violation. *Journal of Geophysical Research*, 75(28), 5351–5371. https://doi.org/10.1029/JA075i028p05351
- Lanzerotti, L. J., & Morgan, C. G. (1973). ULF geomagnetic power near L = 4: 2. Temporal variation of the radial diffusion coefficient for relativistic electrons. *Journal of Geophysical Research*, 78(22), 4600–4610, https://doi.org/10.1029/JA078i022p04600
- Lanzarotti, L. J., Roberts, C. S., & Brown, W. L. (1969). Temporal variations in the electron flux at synchronous altitudes. *Journal of Geophysical*
- Research, 72(23).

  Lanzerotti, L. J., Webb, D. C., & Arthur, C. W. (1978). Geomagnetic field fluctuations at synchronous orbit 2. Radial diffusion. *Journal of*
- Geophysical Research, 83(A8), 3866–3870. https://doi.org/10.1029/JA083iA08p03866

  Lejosne, S., Boscher, D., Maget, V., & Rolland, G. (2013). Deriving electromagnetic radial diffusion coefficients of radiation belt equatorial particles for different levels of magnetic activity based on magnetic field measurements at geostationary orbit. Journal of Geophysical Research: Space Physics. 118, 3147–3156. https://doi.org/10.1002/jgra.50361
- Li, X., Roth, I., Temerin, M., Wygant, J. R., Hudson, M. K., & Blake, J. B. (1993). Simulation of the March 9, 1985 prompt energization and transport of radiation belt particles during the March 24, 1991 SSC. *Geophysical Research Letters*, 20, 2423–2426. https://doi.org/10.1029/93g102701
- Li, Z., Hudson, M., Paral, J., Wiltberger, M., & Turner, D. (2016). Global ULF wave analysis of radial diffusion coeffcients using a global MHD model for the 17 March 2015 storm. Journal of Geophysical Research: Space Physics, 121, 6196–6206. https://doi.org/10.1002/2016JA022508
- Loto'aniu, T. M., Mann, I. R., Ozeke, L. G., Chan, A. A., Dent, Z. C., & Milling, D. K. (2006). Radial diffusion of relativistic electrons into the radiation belt slot region during the 2003 Halloween geomagnetic storms. *Journal of Geophysical Research*, 111, A04218. https://doi.org/10.1029/2005JA011355
- Loto'aniu, T. M., Singer, H. J., Waters, C. L., Angelopoulos, V., Mann, I. R., Elkington, S. R., & Bonnell, J. W. (2010). Relativistic electron loss due to ultralow frequency waves and enhanced outward radial diffusion. *Journal of Geophysical Research*, 115, A12245. https://doi.org/10.1029/2010JA015755
- Mann, I. R., Milling, D. K., Rae, I. J., Ozeke, L. G., Kale, A., Kale, Z. C., et al. (2008). The upgraded CARISMA magnetometer array in the THEMIS era. Space Science Reviews, 141, 413–451. https://doi.org/10.1007/s11214-008-9457-6
- Mann, I. R., Ozeke, L. G., Murphy, K. R., Claudepierre, S., Turner, D. L., Baker, D. N., et al. (2016). Explaining the dynamics of the ultra-relativistic third Van Allen radiation belt. *Nature Physics*, 12, 978–983. https://doi.org/10.1038/nphys3799
- Mauk, B. H., Fox, N. J., Kanekal, S. G., Kessel, R. L., Sibeck, D. G., & Ukhorskiy, A. (2013). Science objectives and rationale for the radiation belt storm probes mission. *Space Science Reviews*, 179, 3–27. https://doi.org/10.1007/s11214-012-9908-y
- O'Brien, T. P. (2015). The activity and radial dependence of anomalous diffusion by pitch angle scattering on split magnetic drift shells. *Journal of Geophysical Research: Space Physics*, 120, 328–343. https://doi.org/10.1002/2014JA020422
- Olson, W. P., & Pfitzer, K. A. (1977). Magnetospheric magnetic field modeling. Annual Scientific eport, Air Force Office of Scientific Research contract F44620-75-C-0033. McDonnell Douglas Astronautics Co.
- Ozeke, L. G., Mann, I. R., Claudepierre, S. G., Henderson, M., Morley, S. K., Murphy, K. R., et al. (2019). The March 2015 superstorm revisited: Phase space density profiles and fast ULF wave diffusive transport. *Journal of Geophysical Research: Space Physics*, 124, 1143–1156. https://doi.org/10.1029/2018JA026326
- Ozeke, L. G., Mann, I. R., Dufresne, S. K. Y., Olifer, L., Morley, S. K., Claudepierre, S. G., et al. (2020). Rapid outer radiation belt flux dropouts and fast acceleration during the March 2015 and 2013 storms: The role of ULF wave transport from a dynamic outer boundary. *Journal of Geophysical Research: Space Physics*, 125, e2019JA027179. https://doi.org/10.1029/2019JA027179
- Ozeke, L. G., Mann, I. R., Murphy, K. R., Jonathan Rae, I., & Milling, D. K. (2014). Analytic expressions for ULF wave radiation belt radial diffusion coefficients. *Journal of Geophysical Research: Space Physics*, 119, 1587–1605. https://doi.org/10.1002/2013JA019204
- Ozeke, L. G., Mann, I. R., Murphy, K. R., Rae, I. J., Milling, D. K., Elkington, S. R., et al. (2012). ULF wave derived radiation belt radial diffusion coefficients. *Journal of Geophysical Research*, 117, A04222. https://doi.org/10.1029/2011JA017463

O'BRIEN ET AL. 18 of 19

- Ozeke, L. G., Mann, I. R., Murphy, K. R., Sibeck, D. G., & Baker, D. N. (2017). Ultra-relativistic radiation belt extinction and ULF wave radial diffusion: Modeling the September 2014 extended dropout event. *Geophysical Research Letters*, 44, 2624–2633. https://doi.org/10.1002/2017GL072811
- Patel, M., Li, Z., Hudson, M., Claudepierre, S., & Wygant, J. (2019). Simulation of prompt acceleration of radiation belt electrons during the 16 July 2017 storm. *Geophysical Research Letters*, 46, 7222–7229. https://doi.org/10.1029/2019GL083257
- Reeves, G. D., Chen, Y., Cunningham, G. S., Friedel, R. W. H., Henderson, M. G., Jordanova, V. K., et al. (2012). Dynamic radiation environment assimilation model: DREAM. Space Weather, 10, S03006. https://doi.org/10.1029/2011SW000729
- Reeves, G. D., McAdams, K. L., Friedel, R. H. W., & O'Brien, T. P. (2003). Acceleration and loss of relativistic electrons during geomagnetic storms. Geophysical Research Letters, 30, 1529. https://doi.org/10.1029/2002GL016513
- Riley, P., & Wolf, R. A. (1992). Comparison of diffusion and particle drift descriptions of radial transport in the Earth's inner magnetosphere. Journal of Geophysical Research, 97(A11), 16865. https://doi.org/10.1029/92ja01538
- Sandhu, J. K., Rae, I. J., Wygant, J. R., Breneman, A. W., Tian, S., Watt, C. E. J., et al. (2021). ULF wave driven radial diffusion during geomagnetic storms: A statistical analysis of Van Allen Probes observations. *Journal of Geophysical Research: Space Physics*, 126, e2020JA029024. https://doi.org/10.1029/2020JA029024
- Sarris, T. E., Li, X., & Temerin, M. (2006). Simulating radial diffusion of energetic (MeV) electrons through a model of fluctuating electric and magnetic fields. *Annales Geophysicae*, 24, 1–2598. https://doi.org/10.5194/angeo-24-2583-2006
- Sarris, T. E., Li, X., Temerin, M., Zhao, H., Khoo, L. Y., Turner, D. L., et al. (2020). Simulations of electron flux oscillations as observed by MagEIS in response to broadband ULF waves. *Journal of Geophysical Research: Space Physics*, 125, e2020JA027798. https://doi.org/10.1029/2020JA027798
- Sarris, T. E., Li, X., Zhao, H., Khoo, L. Y., Liu, W., & Temerin, M. A. (2021). On the association between electron flux oscillations and local phase space density gradients. *Journal of Geophysical Research: Space Physics*, 126, e2020JA028891. https://doi.org/10.1029/2020JA028891 Schulz, M. (1991). The magnetosphere. *Geomagnetism*, 4, 87–293. https://doi.org/10.1016/b978-0-12-378674-6.50008-x
- Schulz, M., & Lanzerotti, L. J. (1974). Physics and chemistry in space. In Particle diffusion in the radiation belts (Vol. 7). Springer.
- Shprits, Y. Y., & Thorne, R. M. (2004). Time dependent radial diffusion modeling of relativistic electrons with realistic loss rates. Geophysical Research Letters, 31, L08805. https://doi.org/10.1029/2004g1019591
- Shprits, Y. Y., Thorne, R. M., Friedel, R., Reeves, G. D., Fennell, J., Baker, D. N., & Kanekal, S. G. (2006). Outward radial diffusion driven by losses at magnetopause. *Journal of Geophysical Research*, 111, A11214. https://doi.org/10.1029/2006ja011657
- Sorathia, K. A., Ukhorskiy, A. Y., Merkin, V. G., Fennell, J. F., & Claudepierre, S. G. (2018). Modeling the depletion and recovery of the outer radiation belt during a geomagnetic storm: Combined MHD and test particle simulations. *Journal of Geophysical Research: Space Physics*, 123, 5590–5609, https://doi.org/10.1029/2018JA025506
- Southwood, D. J., & Kivelson, M. G. (1981). Charged particle behavior in low-frequency geomagnetic pulsations 1. Transverse waves. *Journal of Geophysical Research*, 86(A7), 5643–5655, https://doi.org/10.1029/JA086iA07p05643
- Spence, H. E., Reeves, G. D., Baker, D. N., Blake, J. B., Bolton, M., Bourdarie, S., et al. (2013). Science goals and overview of the radiation belt storm probes (RBSP) energetic particle, composition, and thermal plasma (ECT) suite on NASA's Van Allen probes mission. Space Science Reviews, 179(1–4), 311–336. https://doi.org/10.1007/s11214-013-0007-5
- Su, Z., Xiao, F., Zheng, H., & Wang, S. (2011). Radiation belt electron dynamics driven by adiabatic transport, radial diffusion, and wave-particle interactions. *Journal of Geophysical Research*, 116, A04205. https://doi.org/10.1029/2010JA016228
- Subbotin, D. A., & Shprits, Y. Y. (2009). Three-dimensional modeling of the radiation belts using the Versatile Electron Radiation Belt (VERB) code. Space Weather, 7, \$10001, https://doi.org/10.1029/2008\$W000452
- Teramoto, M., Hori, T., Saito, S., Miyoshi, Y., Kurita, S., Higashio, N., et al. (2019). Remote detection of drift resonance between energetic electrons and ultralow frequency waves: Multisatellite coordinated observation by Arase and Van Allen Probes. Geophysical Research Letters, 46, 11642–11651. https://doi.org/10.1029/2019GL084379
- Tsyganenko, N. A., & Sitnov, M. I. (2005). Modeling the dynamics of the inner magnetosphere during strong geomagnetic storms. *Journal of Geophysical Research*, 110, A03208. https://doi.org/10.1029/2004JA010798
- Tu, W., Cunningham, G. S., Chen, Y., Henderson, M. G., Camporeale, E., & Reeves, G. D. (2013). Modeling radiation belt electron dynamics during GEM challenge intervals with the DREAM3D diffusion model. *Journal of Geophysical Research: Space Physics*, 118, 6197–6211. https://doi.org/10.1002/jgra.50560
- Ukhorskiy, A., & Sitnov, M. (2012). Dynamics of radiation belt particles. In *The Van Allen probes mission* (pp. 545–578). Springer. https://doi.org/10.1007/978-1-4899-7433-4 17
- Ukhorskiy, A. Y., Anderson, B. J., Takahashi, K., & Tsyganenko, N. A. (2006). Impact of ULF oscillations in solar wind dynamic pressure on the outer radiation belt electrons. *Geophysical Research Letters*, 33, L06111, https://doi.org/10.1029/2005GL024380
- Ukhorskiy, A. Y., & Sitnov, M. I. (2008). Radial transport in the outer radiation belt due to global magnetospheric compressions. *Journal of Atmospheric and Solar-Terrestrial Physics*, 70, 1714–1726. https://doi.org/10.1016/j.jastp.2008.07.018
- Zhao, H., Sarris, T. E., Li, X., Weiner, M., Huckabee, I. G., Baker, D. N., et al. (2021). Van Allen Probes observations of multi-MeV electron drift-periodic flux oscillations in Earth's outer radiation belt during the March 2017 event. *Journal of Geophysical Research: Space Physics*, 126, e2021JA029284. https://doi.org/10.1029/2021JA029284
- Zong, Q.-G., Zhou, X.-Z., Wang, Y. F., Li, X., Song, P., Baker, D. N., et al. (2009). Energetic electron response to ULF waves induced by interplanetary shocks in the outer radiation belt. *Journal of Geophysical Research*, 114, A10204. https://doi.org/10.1029/2009JA014393

O'BRIEN ET AL. 19 of 19